A Whole-Cell Screening Platform to Discover Cell Adhesion Molecules that Enable Programmable Bacterial Cell-Cell Adhesion

Po-Yin Chen[1], Yung-Chih Chen[1], Po-Pang Chen[1,2], Kuan-Ting Lin[1,3], Wei-Le Wang[1,3], Kuo-Chiang Hsia[1,2], See-Yeun Ting[1†]

[1]Institute of Molecular Biology, Academia Sinica, Taipei 11529, Taiwan
[2]Institute of Biochemistry and Molecular Biology, College of Life Sciences, National Yang Ming Chiao Tung University, Taipei 11221, Taiwan
[3]Program in Molecular Medicine, National Yang-Ming Chao-Tung University and Academia Sinica, Taipei 11221, Taiwan

[†]Correspondence: syting@gate.sinica.edu.tw

Keywords: bacterial cell adhesion; cell targeting; nanobodies; membrane proteins; synthetic biology

ABSTRACT

Developing programmable bacterial cell-cell adhesion is of significant interest due to its versatile applications. Current methods that rely on presenting cell adhesion molecules (CAMs) on bacterial surfaces are limited by the lack of a generalizable strategy to identify such molecules targeting bacterial membrane proteins in their natural states. Here, we introduce a whole-cell screening platform designed to discover CAMs targeting bacterial membrane proteins within a synthetic bacteria-displayed nanobody library. Leveraging the potency of the bacterial type IV secretion system—a contact-dependent DNA delivery nanomachine—we have established a positive feedback mechanism to selectively enrich for bacteria displaying nanobodies that target antigen-expressing cells. Our platform successfully identified functional CAMs capable of recognizing three distinct outer membrane proteins (TraN, OmpA, OmpC), demonstrating its efficacy in CAM discovery. This approach holds promise for engineering bacterial cell-cell adhesion, such as targeted antimicrobial interventions in the microbiome by deploying programmed inhibitor cells.

INTRODUCTION

Cell-cell interactions are crucial in shaping the intricate structures of microbiomes and facilitating essential functions, including genetic exchange, metabolite transfer, and cellular stress responses. The ability to engineer and manipulate such multicellular arrangements not only enhances our understanding of microbial communities, but also serves as a basis for developing synthetic platforms, which can enable the development of functional microbial consortia with diverse biotechnological applications[3, 4]. For example, multicellular bioconversion represents an area of significant scientific interest, whereby spatially organized microbial communities efficiently convert complex substrates into valuable products[5, 6]. Moreover, drawing inspiration from natural biofilms, self-repairing living biomaterials with cell-cell adhesion properties show regenerative capabilities and display improved resilience[5, 7]. Furthermore, engineered intercellular adhesion could have profound impacts on targeted manipulations within complex microbial populations, enabling precise and efficient interventions against specific bacteria[8-10].

Recent progress in the field of directed cell-cell adhesion has involved the use of bacteria displaying synthetic cell adhesion molecules (CAMs), such as nanobody-antigen or coiled-coil peptide pairs, to facilitate intercellular binding[11, 12]. These strategies are a rational approach for programming multi-microbial materials. However, despite their potential, certain limitations persist due to restrictions in the number of effective binding pairs that can be

53 deployed for cell-cell adhesion purposes. The current development bottleneck arises from using
54 conventional methods to identify potential binders, such as phage- or yeast-display selection,
55 which were not originally designed to identify functional CAMs for bacteria. These methods
56 often present challenges, including 1) poor expression or insufficient display of selected
57 molecules on bacterial surfaces; and 2) reduced binding affinity due to interference from
58 bacterial surface components, such as other membrane proteins or extracellular
59 polysaccharides[8, 9]. Consequently, the laborious process of testing functional CAMs for suitable
60 display on bacterial surfaces is a primary obstacle in the design of engineered microbial
61 communities[11, 12].

62 To address this challenge, we sought to develop a high-throughput screening
63 platform for the identification of functional CAMs with the following properties: *i*) stable
64 display on the bacterial surface; *ii*) targeting of surface antigens in their native conformations;
65 and *iii*) the ability to mediate intercellular adhesions between bacteria. A whole-cell-based
66 platform has the potential to meet these requirements by screening surface-displayed CAMs
67 against bacterial cells harboring target membrane protein antigens. Similar strategies have been
68 implemented to isolate binders against mammalian membrane proteins in their native forms[13,
69 14]. However, analogous platforms for targeting bacterial membrane proteins are limited.

70 In this study, we have developed a directed evolution workflow based on a whole-cell
71 screening approach, aimed at enriching for CAM-displaying cells by using antigen-expressing
72 bacteria as bait. To avoid spontaneous cell aggregates derived from non-specific intercellular
73 binding, our workflow incorporates a positive feedback mechanism at each panning stage,
74 exploiting the contact-dependent DNA delivery nanomachine that operates between interacting
75 bacteria, *i.e.,* the type IV secretion system (T4SS) (**Fig. 1a**). T4SS is a widespread pathway that
76 naturally conjugates genetic material from donor to recipient cells through direct cell-cell
77 interactions. This secretion system is known to target cells with low specificity, unless a strong
78 and stable mating junction forms between bacteria[15]. Elegant works by Robledo *et al*. and Li
79 *et al.* demonstrated that such mating pairs could be achieved by synthetic cell-cell adhesions,
80 promoting target bacterial conjugation even under fluid conditions when cell-cell contacts are
81 transient[9, 10]. Therefore, we posited that the selective properties of T4SS, mediated by synthetic
82 CAMs, could effectively facilitate conjugative transfer of desired genes, such as antibiotic-
83 resistance markers, allowing transconjugants to survive on selective media during the selection
84 process. We anticipated that this approach would result in a positive enrichment for bacteria
85 displaying cognate CAMs from synthetic nanobody libraries (**Fig. 1b**).

86 Here, we demonstrate the application of our whole-cell screening platform to identify
87 functional CAMs that recognize three distinct surface-localized proteins—TraN, OmpA, and
88 OmpC—in their native conformations. We show that mounting these nanobody CAMs on
89 bacterial surfaces not only induces pronounced bacterial cell-cell adhesion, but also enables
90 targeted cell depletion in the microbial community by using programmed inhibitor cells
91 equipped with the nanobodies[8]. By providing a means to engineer tailored interactions between
92 bacteria, our platform opens up new possibilities for the development of advanced synthetic
93 applications in basic research, biotechnology, and clinical settings.
94

95 # RESULTS

96 **Facilitating Selective Gene Transfer in Mixed Populations through Synthetic Cell-Cell**
97 **Adhesion**

98 We began by establishing a selection platform aimed at achieving targeted gene
99 transfers within mixed bacterial populations. This platform relied on the utilization of
100 conjugative donor cells equipped with surface-exposed antigens that could distinguish recipient
101 cells displaying cognate binders from those displaying non-cognate controls. This discerning
102 recognition enabled selective gene transfer events within the mixed population, as depicted in
103 **Figure 1a**. For proof-of-concept experiments, we employed characterized antigen (Ag) -
104 nanobody (Nb) pairs in conjunction with a previously developed intimin display system[11, 16].

105 Our initial assessments involved testing the feasibility of this strategy using *Escherichia*
106 *coli* S17-1 strain (ATCC 47055), a genetically manipulable bacterium with active conjugation
107 ability under standard laboratory conditions. Consistent with previous findings, S17-1 with
108 rigid pili inefficiently transferred antibiotic-resistance markers on mobilizable genetic elements
109 to susceptible recipients in liquid media (**Fig. 1c**), where cell-cell interactions are transient[17,
110 18]. However, the conjugation frequency was significantly enhanced (100- to 1000-fold) when
111 intercellular contacts were enforced by bacterial growth on solid agar plates. The enhancement
112 in conjugation frequency was not observed for an S17-1 strain with a dysfunctional T4SS
113 (Δ*trbE*) for both liquid and solid conditions[19] (**Supplementary Fig. 1a**).

114 Next, we introduced antigen and nanobody expression systems into the conjugative
115 donor and recipient strains, respectively. To enable comparative analyses, we incorporated two
116 distinct characterized cell adhesion binding pairs, namely Ag1-Nb1 and AgInt-NbIB10[11, 20].
117 Conjugation frequencies of S17-1 were markedly increased in liquid cultures when recipient
118 cells displayed cognate nanobodies, whereas only mild effects were detected for non-cognate
119 nanobodies (**Fig. 1d**). Importantly, this selective gene transfer phenomenon was contingent on

120 T4SS being functional within the S17-1 strain (**Supplementary Fig. 1b**). These results support
121 the notion that Ag-Nb-mediated cell-cell adhesion plays an important role in directing the T4SS
122 toward recipient cells when cell-cell interactions are unstable in liquid culture.
123
124 **Iterative Selection Enables Discriminative Enrichment for Low-Abundance Bacteria**
125 **Displaying Cognate Nanobodies**
126 A hallmark of our devised workflow is its capacity to differentially interact with target
127 and non-target cells. To explore this feature further, we subjected antigen (Ag1)-displaying
128 conjugative bacteria to recipient cells expressing matched nanobodies (Nb1) across varying
129 degrees of dilution in the presence of cells expressing a non-matched control. Under these
130 conditions, we detected an enhanced conjugation frequency to recipients when control cells
131 outnumbered target cells by factors of 10-, 100-, and 1,000-fold (**Fig. 2a**). The enrichment for
132 cells expressing matched nanobodies (Nb1) was further verified by diagnostic PCR and
133 sequencing (**Supplementary Fig. 2a,b**). However, we noted that when the target cells were
134 diluted 10,000-fold in the initial pool, no statistically significant difference in conjugation
135 frequency was observed, indicating an upper limit for this discriminant capability (**Fig. 2a**).
136 Central to our selection strategy is the screening of a library comprising a minimum of
137 10^7 distinct nanobody clones. Given this objective, we postulated that iterative rounds of bio-
138 panning could overcome the dilution threshold. Therefore, we harvested transconjugants from
139 the first round of selection and introduced them to a new round of conjugation and selection,
140 using distinct mobilizable antibiotic-resistance markers (**Fig. 2b**). After two rounds of selection,
141 transconjugants having matched nanobody (Nb1) were enriched from a pool of cells initially
142 mixed at a ratio of $1:10^5$ (Nb1:null) (**Fig. 2c and Supplementary Fig. 2c**), and three rounds of
143 bio-panning resulted in successful isolation from a population of cells initially mixed at a ratio
144 of $1:10^7$ (Nb1:null) (**Fig. 2d and Supplementary Fig. 2d**). These outcomes demonstrate the
145 capacity of our designed workflow to exhibit notable specificity towards low-abundance target
146 cells within mixed bacterial populations.
147
148 **Discovery of a Nanobody Targeting the Natural Adhesin TraN**
149 Building on the success of our selection workflow, next we sought to determine if our
150 approach could yield nanobody clones capable of targeting protein antigens naturally present
151 on bacterial cell surfaces. We were particularly interested in TraN, a bacterial outer-membrane
152 protein with accessible epitopes on the cell surface that is involved in stabilizing mating pairs
153 and facilitating horizontal gene transfers[15, 21]. Most relevant to our study, TraN functions as a

154 natural adhesin, promoting cell-cell adhesion upon binding to its specific receptor. This
155 property renders it an ideal module for enabling programmable cell-cell adhesion and
156 represents an appropriate choice for our proof-of-principle experiments.

157 Accordingly, we assessed the feasibility of isolating bacteria expressing cognate
158 nanobodies from a mixed population by displaying the TraN antigen on S17-1 conjugative cells.
159 Our experimental workflow encompassed incubating of S17-1 cells with a bacteria-displayed
160 nanobody library derived from a synthetic pool comprising approximately 10^7 clones of distinct
161 nanobodies[22]. Following each round of selection, we harvested colonies and conducted high-
162 throughput sequencing to confirm enrichment. Our analyses revealed a progressive increase in
163 the abundance of specific nanobody clones within the library pool across successive rounds of
164 selection (**Fig. 3a and Supplementary Table 3**). To validate TraN-dependent cell-cell
165 adhesion, we selected the top three unique sequences from the final round of panning,
166 introduced them to model *E. coli*, and conducted a macroscopic cell aggregation assay using
167 optical density (OD_{600}) measurements to quantify the binding strength and specificity between
168 cells[11]. If the nanobodies possessed CAM capacity, we expected to observe rapid precipitation
169 in a cell mixture of the corresponding nanobody- and antigen-displaying strains. Consistent
170 with our screening results, we observed a significant reduction in supernatant OD_{600} in a
171 mixture of cells expressing one of the top nanobodies and cells displaying TraN, indicating that
172 the specific nanobody on the cell surface served as a functional CAM in binding to TraN and
173 precipitating cells from culture (**Fig. 3b and Supplementary Fig. 3a**). This result prompted us
174 to pursue an in-depth characterization of the isolated TraN-specific nanobody, hereafter
175 referred to as Nb^{traN} (**Fig. 3c**).

176 As expected, we detected a stable interaction between purified Nb^{traN} and the surface-
177 exposed domain of TraN ($TraN^{surf}$) via size-exclusion chromatography (**Supplementary Fig.
178 3b,c**). Further analysis revealed a binding affinity (K_D) of 4.45 μM between Nb^{traN} and $TraN^{surf}$
179 (**Fig. 3d,e**), confirming the specificity of the interaction. To gain insights into the interaction
180 between Nb^{traN} and TraN, as well as how it promotes cell-cell adhesion in bacterial mixtures,
181 we determined a 3.67 Å X-ray crystal structure of Nb^{traN} in complex with $TraN^{surf}$ (PDB: 8X7N)
182 (**Fig. 3f,g and Supplementary Table 1**). The Nb^{traN}/$TraN^{surf}$ complex structure was determined
183 by molecular replacement using nanobody homolog, Nb.b201, as a search model, which has
184 an identical fixed framework region to that of Nb^{traN} (PDB: 5VNV)[22]. In our structure, Nb^{traN}
185 and $TraN^{surf}$ share an extensive interaction surface consisting of two contact regions that are
186 primarily formed by the complementarity-determining regions 2 and 3 of Nb^{traN} (CDR2, CDR3)
187 (**Fig. 3f**). In contrast, CDR1, the other variable loop in Nb^{traN}, did not present any direct

188 interaction with $TraN^{surf}$ in our structure. Importantly, the contact interface between Nb^{traN} and
189 $TraN^{surf}$ is rich in non-polar amino acids, suggesting their potential contribution to stable
190 complex formation (**Fig. 3g**). To test this hypothesis, we introduced alanine substitutions into
191 the interacting residues of CDR2 and CDR3 to disrupt the specific interaction, and then
192 conducted macroscopic aggregation assays and isothermal titration calorimetry (ITC) to
193 evaluate their impact on Nb^{traN}/TraN binding. In line with our structural data, we did not
194 observe any cell aggregates for either the CDR2 (F47A/Y58A) or CDR3 (Y98A/L100A)
195 mutants when mixed with cells displaying TraN (**Supplementary Fig. 4a**). These mutants also
196 displayed significantly reduced binding affinities for TraN (**Supplementary Fig. 4b-e**).
197 Together, these data indicate that the hydrophobic residues within two of the CDRs of Nb^{traN}
198 interact with the surface-exposed domain of TraN, facilitating cell-cell adhesion when Nb^{traN}
199 is mounted on bacterial surfaces.
200
201 **Deep Mutational Nanobody Engineering Enhances the Binding Affinity of Nb^{traN} for**
202 **TraN**
203 Although we successfully identified a functional CAM targeting TraN from our
204 nanobody pool, the binding affinity of Nb^{traN} was relatively modest (**Fig. 3d,e**). We postulate
205 that nanobodies of higher affinity may not be present in the original library since the number
206 of unique nanobody sequences was not saturated. This limitation in pool diversity could have
207 impeded the discovery of high-affinity CAMs. Therefore, we set out to directly engineer Nb^{traN}
208 by means of deep mutational scanning in conjunction with our whole-cell screening platform
209 to obtain nanobody variants displaying an improved affinity for TraN (**Fig. 4a**). Our rationale
210 was that if cells expressing the Nb^{traN} variants exhibited an enhanced affinity for TraN, they
211 would acquire selective markers in a higher frequency, resulting in their enrichment within the
212 population during the selection process. As an initial step, we focused on the nanobody's CDR3
213 sequence, given that it is longer than other CDRs and is an important loop for antigen
214 recognition[23]. Accordingly, we generated a focused library by single-site saturation
215 mutagenesis of each residue in the CDR3 of Nb^{traN} using commercially available chip
216 oligonucleotides (14 residues × 19 alternative amino acids/residues = 266 variants in the
217 nanobody pool, as illustrated in **Fig. 4a**). The newly constructed nanobody library was then
218 introduced into *E. coli* consisting of a display system and incubated with S17-1 cells expressing
219 TraN for selection. After a single round of panning, we harvested surviving transconjugants on
220 selective media and subjected them to high-throughput sequencing. We quantified the number

221 of transconjugants by analyzing unique nanobody sequences in the pre- and post-selection
222 populations.
223 To gain a comprehensive understanding of the amino acid variants within the CDR3 of
224 Nb^{traN} that affect conjugation in our screening process, we generated a sequence-function map
225 illustrating variant conjugative scores (**Fig. 4b and Supplementary Fig. 5a**). Compared to
226 wild-type Nb^{traN}, 69% of the variants showed a decrease in conjugation ability following
227 screening, whereas 31% showed an increase. Notably, substitutions of residue Y98 in CDR3
228 with other amino acids resulted in a reduced number of transconjugants in the pool, aligning
229 with our above-described findings regarding its role in mediating the interaction between Nb^{traN}
230 and TraN (**Supplementary Fig. 4**). Several Nb^{traN} variants significantly outperformed wild-
231 type Nb^{traN} in the whole-cell screening platform. We were particularly interested in the cysteine
232 variants located sequentially from residues 101 to 107, all of which elicited a substantial
233 increase in the transconjugant population. These residues are positioned in close proximity to
234 the Nb^{traN}/$TraN^{surf}$ interface in our complex structure (PDB: 8X7N) and have the potential to
235 interact more effectively with TraN upon mutating to cysteine during cell-cell contacts
236 (**Supplementary Fig. 5b**). Again, using macroscopic cell aggregation assays, we confirmed
237 that cells displaying the CDR3 cysteine variants with the highest conjugative score (S105C and
238 H106C) presented precipitation upon mixing with TraN-expressing cells (**Fig. 4c and**
239 **Supplementary Fig. 6a**). To rule out indirect effects related to differences in protein levels,
240 we conducted immunoblotting analysis and did not observe significant increases in protein
241 expression for the cysteine variants relative to wild-type Nb^{traN} (**Fig. 4d**). We further assessed
242 if cells displaying the Nb^{traN} cysteine variants could promote cell-cell adhesion through
243 comparative conjugation in liquid culture. Consistent with the results from our deep-mutational
244 screening, recipients displaying the Nb^{traN} cysteine variants exhibited a more than 5-fold
245 increase in conjugation frequencies when incubated with S17-1 donor cells expressing TraN
246 (**Fig. 4e**). Finally, we purified Nb^{traN}S105C and Nb^{traN}H106C and used ITC to measure their
247 binding affinities for $TraN^{surf}$. Compared to wild-type Nb^{traN}, the cysteine variants presented,
248 on average, a 3-fold increase in binding to $TraN^{surf}$ *in vitro* (**Fig. 4f,g and Supplementary Fig.**
249 **6b,c**). In summary, we have demonstrated that our whole-cell screening platform not only
250 identifies functional CAMs from a synthetic library, but this method is feasible for enhancing
251 the cell adhesion capabilities of those identified CAMs by deploying strategic deep mutational
252 engineering.
253

254 **Discovery of Nanobodies Targeting the Embedded Membrane Proteins OmpA and**
255 **OmpC**

256 Encouraged by the success of our selection method, we set out to identify functional
257 CAMs capable of recognizing embedded membrane proteins. These proteins possess few
258 surface-exposed epitopes and pose challenges for antibody acquisition through conventional
259 screening methods or large-animal immunization (**Supplementary Fig. 7**). We selected two
260 target antigens, OmpA and OmpC, representing two bacterial proteins naturally localized on
261 the outer membrane that exert important roles in maintaining bacterial surface integrity and
262 regulating membrane permeability[24, 25]. To our knowledge, no CAMs targeting the extracellular
263 epitopes of OmpA or OmpC have been reported previously, making nanobodies targeting them
264 especially unique and relevant. It is worth noting that although endogenous OmpA and OmpC
265 are present in the S17-1 conjugative cells, we overexpressed these proteins by introducing an
266 additional gene copy by plasmids, thereby enhancing the likelihood of isolating synthetic
267 binders against these target antigens. Next, we incubated the S17-1 strains ($OmpA^+$ or $OmpC^+$)
268 with the bacteria-displayed nanobody library, with the objective of identifying functional
269 CAMs specifically tailored to these embedded membrane proteins.

270 Following three rounds of bio-panning along with sequencing analyses, we successfully
271 identified nanobodies targeting both of these membrane proteins, which we have designated
272 Nb^{ompA} and Nb^{ompC} (**Fig. 5a**). We found that *E. coli* harboring OmpA and OmpC underwent
273 self-aggregation when they expressed these nanobodies on their surfaces, indicating their
274 potential utility as CAMs (**Fig. 5b**). A comparative conjugation assay in liquid culture
275 supported this notion, as the recipient cells displaying either Nb^{ompA} or Nb^{ompC} on their surfaces
276 presented greatly enhanced conjugation frequencies upon incubation with S17-1 donor cells
277 having OmpA and OmpC antigens (**Fig. 5c,d**). Finally, to validate the binding capacity of
278 Nb^{ompA} and Nb^{ompC} to their corresponding surface antigens, we explored their potential utility
279 as reagents for immunofluorescence labeling. We fused these nanobodies in-frame with a green
280 fluorescent protein, referred to as Nb-GFP, purified them, and then performed a standard cell
281 labeling procedure for visualization by fluorescence microscopy (**Fig. 5e,f and**
282 **Supplementary Fig. 8**). We observed distinct fluorescence signals colocalized with wild-type
283 *E. coli* hosting endogenous OmpA and OmpC when bound with Nb^{ompA}-GFP and Nb^{ompC}-GFP,
284 respectively. These signals diminished when the Nb-GFPs were incubated with mutant *E. coli*
285 strains (Δ*ompA*, Δ*ompC*). These results not only evidence the binding capacity of the Nb-GFPs
286 toward their cognate membrane antigens, but also highlight the potential utility of CAMs for
287 detecting bacteria expressing desired surface proteins.

288

289 **Nanobody-Programmed Inhibitor Cells Selectively Deplete Target Bacteria from Mixed**
290 **Populations**

291 One emerging and valuable application of synthetic CAMs is targeted antimicrobial
292 interventions[8, 10]. We recently developed programmed inhibitor cells (PICs) displaying surface
293 nanobodies that can selectively eliminate *E. coli* expressing cognate surface antigens within
294 complex microbial communities, leveraging the potent antibacterial activity of the type VI
295 secretion system (T6SS) in *Enterobacter cloacae*[26, 27] (**Fig. 6a**). Despite being an important
296 advance, the nanobodies employed in prior studies that recognize the embedded membrane
297 protein BamA can be hindered by bacterial surface structures such as lipopolysaccharides
298 (LPS)[8, 28]. Taking advantage of our newly identified CAMs, next we endeavored to determine
299 if Nb^{ompA} and Nb^{ompC} are compatible with PICs for targeted cell elimination in bacterial
300 mixtures. More importantly, we wanted to determine if PICs equipped with these nanobodies
301 could selectively kill *E. coli* without altering native surface structures.

302 We proceeded to generate PICs displaying nanobodies that target OmpA and OmpC,
303 denoted $PIC^{Nb\text{-}OmpA}$ and $PIC^{Nb\text{-}OmpC}$, respectively. To examine their capacity to direct the
304 antibacterial activity of PICs against target *E. coli*, we performed target depletion assays using
305 a high cell density and short timescale to mimic natural microbial communities found in the
306 environment or host. Indeed, we found that both $PIC^{Nb\text{-}OmpA}$ and $PIC^{Nb\text{-}OmpC}$ effectively reduced
307 the cell viability of *E. coli* within an hour by more than an order of magnitude ($PIC^{Nb\text{-}OmpA}$,
308 27.7-fold; $PIC^{Nb\text{-}OmpC}$, 168.2-fold), in a manner dependent on the presence of respective
309 nanobodies, the T6SS, and the corresponding antigens on target cells (**Fig. 6b-d and**
310 **Supplementary Fig. 9**). In contrast, PICs equipped with nanobody targeting BamA ($PIC^{Nb\text{-}}$
311 ^{BamA}) exerted a minimal impact on wild-type *E. coli* CFU numbers, unless LPS were truncated[8]
312 (**Fig. 6e and Supplementary Fig. 9**). These results provide evidence for the compatibility of
313 both Nb^{ompA} and Nb^{ompC} with PICs to achieve targeted cell depletion. Moreover, we have
314 showcased examples of specific antimicrobial interventions with minimal perturbation of the
315 target cells. Lastly, to assess the feasibility of $PIC^{Nb\text{-}OmpA}$- and $PIC^{Nb\text{-}OmpC}$-mediated targeting
316 within complex bacterial mixtures, we isolated total fecal bacteria from conventionally reared
317 mice, which contain wild-type *E. coli* targets. We measured the capacity of $PIC^{Nb\text{-}OmpA}$ and
318 $PIC^{Nb\text{-}OmpC}$ to selectively deplete *E. coli* from this diverse and undefined microbiome. Within
319 60 minutes post-PIC addition, *E. coli* CFU levels dropped significantly by 92% ($PIC^{Nb\text{-}OmpA}$)
320 or 78% ($PIC^{Nb\text{-}OmpC}$), whereas PICs displaying Nb^{BamA} ($PIC^{Nb\text{-}BamA}$) had no observable impact
321 on survival of the target cells (**Fig. 6f and Supplementary Fig. 10**). This outcome underscores

322 the potential of PIC-mediated targeting as a robust approach for selectively depleting target
323 cells from complex microbial communities.
324

325 **DISCUSSION**

326 Cell adhesion molecules are important in the study of fundamental biology and
327 represent promising biotechnological tools. However, a key issue is how to identify functional
328 CAMs that effectively mediate intercellular assemblies for desired outcomes. In this study, we
329 report our development of a whole-cell screening platform designed to discover CAMs that
330 facilitate programmable bacteria-bacteria adhesion. The success of this platform relies on a
331 strategic combination of functional and positive selection, leveraging the T4SS for contact-
332 dependent DNA delivery. The T4SS serves as a discriminatory enrichment tool, selectively
333 favoring bacteria displaying functional CAMs, thereby addressing limitations associated with
334 conventional methods. Our successful identification of nanobodies targeting outer membrane
335 proteins attests to the effectiveness of our approach. The nanobodies isolated in this study
336 exhibit stable and specific interactions with their cognate target antigens, underscoring their
337 potential as versatile tools for engineering bacteria-bacteria adhesions. These CAMs present
338 opportunities for future applications, such as engineering complex multi-component metabolic
339 pathways and biomaterials[5-7], as well as precision-targeted manipulation[8, 10]. Furthermore, we
340 anticipate our method will prove compatible with existing cell-cell adhesion platforms,
341 enabling the design and fine-tuning of multicellular assemblies, patterns, and morphologies,
342 thereby positioning CAMs as key components in the synthetic microbiology toolkit[11, 12].

343 Our study primarily serves to demonstrate the platform design and provide proof-of-
344 concept applications, yet we recognize the potential for further optimization with a view toward
345 specific targets. For example, we detected basal DNA conjugation frequencies in the absence
346 of CAMs (0.01-0.001%, as shown in **Fig. 1 and 2**), indicating avenues for improvement. Our
347 future efforts will concentrate on identifying or engineering alternative conjugative cells to
348 maximize specific gene transfer efficiency while minimizing non-specific cell-cell adhesion.
349 Importantly, the flexibility of our whole-cell screening platform, as exemplified through deep
350 mutational engineering (**Fig. 4**), establishes a foundation for future endeavors aimed at
351 expanding CAM diversity. Incorporating a more extensive and diverse pool of CAMs promises
352 broader applicability and functionalities. Lastly, to extend the scope for identifying functional
353 CAMs, future studies could explore alternative screening platforms utilizing Gram-positive
354 bacteria, enabling the targeting of membrane antigens beyond the Gram-negatives examined
355 herein. Despite divergences in DNA transfer mechanisms, the presence of conjugation

356 machinery in Gram-positive bacteria supports the feasibility of extending contact-dependent
357 DNA transfer via synthetic cell-cell adhesion[29].
358 Despite the primary goal of this study being to develop a platform for isolating CAMs
359 between bacteria, we envision that the principles of selection we deployed can transcend this
360 specific scope. One notable advantage of our selection design is that by exploiting cell surface
361 display systems to present antigens of interest. We have overcome technical challenges
362 associated with recombinant protein purification in conventional screening platforms[14, 22].
363 Numerous bacterial surface display systems have been developed in recent decades, which can
364 efficiently express heterologous proteins for various purposes[30]. We anticipate that our rapid
365 whole-cell-based selection regime can be extended to isolate antigen-specific binders using
366 those protein display systems.
367 Our study not only demonstrates how functional CAMs can be identified via a high-
368 throughput screening workflow, but also showcases their compatibility with existing
369 technologies relying on cell-cell adhesion. By installing isolated CAMs targeting OmpA or
370 OmpC on the surface of PICs, we could specifically direct the antibacterial activity of PICs
371 toward target bacteria in mixed populations (**Fig. 6**). Overall, our results herein highlight the
372 vast potential of our screening platform and its potential integration with other synthetic
373 biology tools. For instance, we envisage additional possibilities using CRISPR-based systems
374 or engineered antimicrobials[10, 31-33]. Combining different synthetic biology approaches for the
375 precise manipulation of microbial communities could yield synergistic benefits with diverse
376 applications. The adaptability and versatility of CAMs identified using our platform offer
377 opportunities for innovation, both in terms of navigating the challenges posed by biological
378 system complexity and deciphering potential applications. In conclusion, this study sheds light
379 on the transformative potential of CAMs in microbiology and synthetic biology.
380

381 # METHODS

382 **Bacteria, Yeast, and Culture Conditions**

383 The strains utilized in this study are detailed in **Supplementary Table 2**. We used the
384 following *Escherichia coli* strains: S17-1 ATCC 47055 to display antigens of interest and
385 transfer plasmids containing distinct antibiotic-resistance markers for the selection method;
386 MG1655 to display nanobodies and validate nanobody-binding specificity; DH5α and PIR1 in
387 cloning and plasmid maintenance; S17-1 λ pir for conjugal transfer of pRE118 plasmid into *E.*
388 *coli*; and BL21 (DE3) pRIL for overproduction and purification of protein samples.
389 *Enterobacter cloacae* ATCC-13047 was utilized for target depletion assays[8]. All bacteria were

390 routinely cultured at 37 °C in Luria Bertani (LB) medium unless noted otherwise. The yeast-
391 display nanobody library was recovered by growing it in Yglc4.5 –Trp medium at 30 °C in a
392 shaker[22]. Antibiotics and chemicals were used at the following concentrations: 50 μg/mL
393 streptomycin; 150 μg/mL carbenicillin; 50 μg/mL kanamycin; 25 μg/mL chloramphenicol; 15
394 μg/mL gentamicin; 100 μg/mL trimethoprim; 500 ng/mL anhydrotetracycline (aTc); 100 μM
395 isopropyl β-D-1-thiogalactopyranoside (IPTG); 1% (*w/v*) L-(+)-arabinose; and 200 mM
396 sucrose.
397
398 **Mice**
399 Fecal samples from three male wild-type C57BL/6J mice were utilized in this study.
400 Care and maintenance of these mice were conducted according to the protocol of the
401 Institutional Animal Care and Use Committee (IACUC) of the Institute of Molecular Biology
402 (Academia Sinica, Taiwan) and approved by its Animal Center, where the mice were bred and
403 housed. All mice were maintained under controlled light conditions (12-hour light-dark cycle)
404 with access to standard food and water. Prior to oral gavage with wild-type *E. coli* MG1655
405 targets, the mice underwent a 4-hour fasting period.
406
407 **Plasmid Construction**
408 The plasmids and primers utilized in our study are listed in **Supplementary Table 2**.
409 Tet expression plasmids, which were used for nanobody display on the surface of both *E. coli*
410 and *E. cloacae*, were derived from pDSG323-based expression plasmids as described
411 previously[8, 11]. The TraN antigen expression plasmid (pDSG-TraN) was constructed by
412 polymerase chain reaction (PCR) amplification and subsequent cloning of the *traN* gene
413 (AAL23498.1) from the pSLT plasmid of *Salmonella* Typhimurium LT2 strain into pDSG323
414 at the *NotI* and *PstI* restriction sites. The OmpA and OmpC arabinose-inducible plasmids
415 (pBAD18-OmpA, pBAD18-OmpC) were generated by PCR amplification and subsequent
416 cloning of the respective genes (NP_415477.1, NP_416719.1) from the genomic DNA of *E.*
417 *coli* MG1655 strain into the *SacI* and *XbaI* restriction sites of pBAD18. A Myc-tag sequence
418 (EQKLISEEDL) was introduced at the C-terminus of Nb^{traN} and its variants by means of site-
419 directed mutagenesis[34].
420 For the $TraN^{surf}/Nb^{traN}$ complex purification constructs, the sequences were amplified
421 and cloned into multiple cloning site (MCS)-1 (*BamH1* and *NotI* sites) and MCS-2 (*NdeI* and
422 *XhoI* sites) of pETDuet-1, respectively, resulting in fusion of an N-terminal hexa-histidine to
423 $TraN^{surf}$. Purification of Nb^{traN}, Nb^{ompA}, and Nb^{ompC} involved amplifying their sequences and

424 cloning them into the MCS (*NdeI* and *XhoI* sites) of pET22b, fused with a C-terminal hexa-
425 histidine tag. Nb^{traN} nanobody variants were introduced into the expression plasmids using site-
426 directed mutagenesis[34]. The Nb^{ompA}-GFP and Nb^{ompC}-GFP constructs were generated by PCR
427 amplification of the GFP sequence from pET11a-GFP-avi and inserting it between the
428 nanobody sequences and the hexa-histidine tag at the C-terminus of pET22b plasmids via
429 Gibson assembly[35]. To purify $TraN^{surf}$ alone, the sequence was amplified and cloned into MCS-
430 1 (*BamH1* and *NotI* sites) of pETDuet-1, generating a fusion construct with an N-terminal hexa-
431 histidine tag. The *E. coli ompW* in-frame deletion plasmid (pRE118_EcoliΔompW) was
432 generated by utilizing the suicide vector pRE118[36]. We amplified 750 bp regions flanking the
433 deletion, joined them by means of splicing by overlap extension (SOE) PCR, and subsequently
434 cloned them into pRE118 at the *SacI* and *XbaI* restriction sites. For mobilizable plasmids with
435 distinct antibiotic-resistance genes, the pGenR was created from plasmid pPSV37 by deleting
436 the T7-expression system and re-ligating the vector by means of Gibson assembly[37], whereas
437 pTmpR was created from plasmid pSCrhaB2 by deleting the rhamnose-expression system[38].
438 The pUC18T-mini-Tn7T plasmid consists of an ampicillin-resistance gene and its oriT was
439 renamed as pAmpR for the purposes of our study[39].
440
441 **Genetic Manipulation**
442 We used the lambda red recombinase system to generate *E. coli* strains in which *ompA*,
443 *ompC*, or *trbE* had been deleted[40]. In brief, PCR products comprising a kanamycin resistance
444 cassette from pKD4, flanked by 50~100 bp homologous to the 5' and 3' termini of these genes,
445 were electroporated into *E. coli* strains (MG1655 or S17-1) carrying pKD46 and induced by
446 arabinose for 5 hours at 30 °C to express the recombinase. Subsequently, *E. coli* was incubated
447 in LB for 1 hour, plated on chloramphenicol-containing LB agar, and incubated overnight at
448 37 °C. To remove the kanamycin resistance cassette from *E. coli*, pCP20 plasmid hosting the
449 FLP recombinase gene was transformed into the deletion strains, which were then grown at 30
450 °C on carbenicillin-containing LB agar. A single colony was picked and inoculated into LB
451 media at 43 °C to select for loss of pCP20.
452 To delete *ompW* from *E. coli* MG1655, pRE118_EcoliΔompW was transformed into *E.*
453 *coli* S17-1 λ pir. The donor cells carrying the deletion construct and *E. coli* MG1655 were
454 grown overnight on LB plates containing antibiotics, as appropriate. The cells were then
455 scraped together to create a 2:1 donor-recipient mixture, which was spread out on an LB agar
456 plate and incubated at 37 °C for 6 hours to facilitate plasmid transfer via conjugation. Cell
457 mixtures were then scraped into LB and plated onto LB medium agar plates supplemented with

458 kanamycin and chloramphenicol to select for *E. coli* containing the chromosomally inserted
459 deletion construct. The *E. coli* merodiploid strains were grown overnight in non-selective LB
460 medium at 37 °C, followed by counter-selection on LB low salt plates containing sucrose.
461 Kanamycin-sensitive colonies were screened for allelic replacement by colony PCR and
462 mutations were confirmed by Sanger sequencing of the PCR products.
463
464 **Bacterial Conjugation Assays**
465 For conjugation assays, the conjugative strain *E. coli* S17-1 ATCC 47055 was employed
466 as the donor carrying transferable plasmids with selection markers, whereas *E. coli* MG1655
467 served as the recipient. Overnight bacterial cultures were centrifuged at 21,100 x *g* for 1 minute
468 to pellet the cells, followed by the removal of the culture supernatant. The cells then underwent
469 a single wash in LB broth and were subsequently resuspended in LB broth. The donor and
470 recipient cells were adjusted to OD_{600} = 0.005 and 0.0025, respectively. Liquid conjugation
471 assays involved incubating cell mixtures at 37 °C with continuous agitation at 200 rpm for 6
472 hours. For conjugation assays on solid media, cell mixtures were spotted onto LB agar plates
473 and incubated at 37 °C for 6 hours. Following incubation, the cells were collected, serially
474 diluted, and plated on selective media to quantify colony-forming units (CFUs). Three
475 transferable plasmids contained gentamicin-, ampicillin-, or trimethoprim-resistance genes,
476 respectively. The recipient strain was marked by chromosomal insertion of a chloramphenicol-
477 resistance gene, whereas the donor strains remained unmarked. The total recipient population
478 was assessed by enumerating CFUs on LB plates containing chloramphenicol. The count of
479 transconjugant populations was determined by enumerating CFUs on LB plates with
480 chloramphenicol, which also contained the relevant resistance markers (gentamicin, ampicillin,
481 or trimethoprim), depending on the specific conjugative plasmid employed in the selection
482 process.
483
484 **Ag/Nb Mismatch Conjugation Experiment**
485 We used four different mixed cell cultures in the mismatch conjugation assay.
486 Conjugative *E. coli* S17-1 strains displaying either Ag1 or AgInt from Tet expression plasmids
487 were co-cultured with recipient strains displaying Nb1 or NbIB10 from Tet expression plasmids.
488 Initial cell concentrations for donor and recipient strains were set to OD_{600} = 0.005 and 0.0025,
489 respectively. Following 6-hour incubation in a liquid medium containing kanamycin and aTc
490 with continuous shaking at 37 °C, the cells were subjected to serial dilution and plated on
491 selective media to quantify CFUs as described above.

492 To assess if the whole-cell screening approach exhibits specificity toward low-
493 abundance target cells within mixed bacterial populations, overnight cell cultures were
494 centrifuged at 21,100 x *g* for 1 minute. The culture supernatant was discarded, and the cell
495 pellet was collected. After a single wash, cells were resuspended in LB broth, and their
496 concentration was adjusted to OD_{600} = 1.0. Recipient cells expressing Nb1 and Null were mixed
497 at varying ratios (10^1- to 10^7-fold dilutions as specified). The recipient mixture and donor cells
498 displaying Ag1 were diluted to OD_{600} = 0.0025 and 0.005, respectively. The assay comprised
499 three rounds of bio-panning. In the initial round, the donor strain carrying a transferable
500 gentamicin resistance gene was utilized. Following 6-hour incubation at 37 °C with shaking at
501 200 rpm, cultures were diluted and plated on selective media for CFU quantification. The
502 remaining culture was plated on selective media to initiate the next panning round. After 16
503 hours of incubation at 37 °C, recipient colonies that grew on selective plates were harvested
504 and resuspended in LB broth for the second panning round. The recipient culture and the donor
505 carrying a transferable ampicillin resistance gene were diluted to OD_{600} = 0.0025 and 0.005,
506 respectively. After incubation again at 37 °C with agitation at 200 rpm for 6 hours, cultures
507 were diluted and plated on selective media for CFU quantification. The remainder of the culture
508 was plated on selective media for the subsequent panning round. Following another 16 hours
509 of incubation at 37 °C, recipient colonies that grew on the selective plates were harvested and
510 resuspended in LB broth for the third panning round. The recipient culture and the donor
511 carrying a transferable trimethoprim resistance gene were diluted to OD_{600} = 0.0025 and 0.005,
512 respectively. After incubation at 37 °C with agitation at 200 rpm for 6 hours, cultures were
513 diluted and plated on selective media for CFU quantification.
514
515 **Bacterial Nanobody Display Library Construction**
516 The bacterial display library used in this study was derived from a yeast nanobody
517 library established in a previous study[22]. Plasmids containing nanobody genes were first
518 extracted from the yeast library, and the nanobody sequences were subsequently amplified via
519 PCR. These fragments were then subcloned into pDSG323 backbone vectors using the Gibson
520 assembly method and chemically transformed into *E. coli* DH5α for plasmid enrichment. A
521 total of fifty separate Gibson assembly reaction products were transformed, resulting in the
522 collection of >10^7 colonies, after which plasmids were extracted and pooled. The bacteria
523 nanobody display library (100 ng) was then transformed into the *E. coli* MG1655 Δ*ompW* strain
524 via electroporation. We selected the Δ*ompW* strain to minimize the interactions between OmpW

525 and TraN, as suggested by Low *et al.*[21, 41]. The cells were harvested and resuspended in LB
526 with 10% glycerol for storage at -80 °C.
527 To construct the Nb^{traN} CDR3 library for deep mutational engineering, 14 sites on
528 CDR3 sequences (AYPLDEIGSHDPHS) underwent mutagenesis, with each site mutated into
529 all desired amino acids using optimal *E. coli* codons. GenScript performed DNA
530 oligonucleotide library synthesis on a programmable column. The pooled mutagenesis library
531 was subsequently cloned into the pDSG323 backbone and transformed into *E. coli* DH5α
532 competent cells. Sanger sequencing was conducted to determine library capacity before
533 colonies were collected, and the plasmids were then extracted. The pool of plasmids was then
534 transformed into the *E. coli* MG1655 Δ*ompW* strain via electroporation, resulting in a collection
535 of >30,000 colonies stored in LB broth with 10% glycerol at -80 °C.
536
537 **Nanobody CAM Isolation using the Whole-Cell Screening Platform**
538 Conjugative *E. coli* S17-1 expressing indicated antigens (TraN, OmpA, or OmpC)
539 along with transferring plasmids containing distinct antibiotic-resistance markers served as the
540 donor strain, whereas the bacterial nanobody library acted as the recipient. In the initial bio-
541 panning round, the donor with a mobilized gentamycin-resistance plasmid and the recipient
542 nanobody display library were both diluted to OD_{600} = 0.05 in LB broth and incubated at 37
543 °C with shaking at 200 rpm until log phase was attained. The donor cells and the library culture
544 were then diluted to OD_{600} = 0.0025 and 0.005, respectively, and co-cultured in LB broth with
545 aTc. After 6-hour incubation at 37 °C with shaking at 200 rpm, the culture was plated on
546 selective media containing gentamycin and chloramphenicol and incubated at 37 °C for 16
547 hours. All colonies (>10^6 clones) were harvested and resuspended in LB broth. In the second
548 round of panning, recipient cells from the first round and donor cells carrying a transferrable
549 ampicillin resistance plasmid were mixed at OD_{600} = 0.0025 and 0.005, respectively. Following
550 the same panning conditions as in the initial round, the culture was plated on selective media
551 containing carbenicillin and chloramphenicol. After 16-hour incubation at 37 °C, all colonies
552 were collected and resuspended in LB broth for the third round of panning. The culture
553 harvested after the second panning round was co-cultured with donor cells carrying a
554 transferrable trimethoprim resistance plasmid at a ratio of OD_{600} = 0.0025 and 0.005,
555 respectively. After 6-hour co-culture under the same conditions as the previous round, the
556 culture was plated on selective media containing trimethoprim and chloramphenicol. All grown
557 colonies were harvested. Cells obtained after each panning round were collected to analyze
558 nanobody diversity at each time point. For Nb^{traN} deep mutational engineering, conjugative *E.*

559 *coli* S17-1 expressing TraN served as the donor strain, and the bacterial Nb^{traN} mutant library
560 served as the recipient. The selection process comprised a single round of bio-panning, as
561 described above.
562
563 **Macroscopic Cell Aggregation Assays**
564 *E. coli* displaying nanobodies or antigens were initially inoculated in LB broth with aTc
565 inducer. Following a 24-hour incubation at 37 °C, the cultures were vortexed and mixed in a
566 1:1 ratio with the indicated testing combination. The cell mixtures were then placed in cuvettes
567 with a 1-cm light path at room temperature. After 24 hours of settling, cultures from the top
568 25% of the wells were collected, and their OD_{600} was measured using a Nano300
569 microspectrophotometer.
570
571 **Protein Purification**
572 His-tagged $TraN^{surf}$ and Nb^{traN} proteins were co-expressed from pET-Duet-1 in *E. coli*
573 BL21 (DE3) pRIL. Stationary phase cultures of expression strains were used to inoculate 1 L
574 of LB broth containing carbenicillin and chloramphenicol. Cells were cultured in a shaking
575 incubator at 37 °C and 220 rpm until they reached log phase (OD_{600} = 0.6~0.8), induced by
576 IPTG, and then incubated at 30 °C and 220 rpm for 18 hours. Cells were harvested by
577 centrifugation at 4 °C and 4,000 x *g* for 20 minutes and then resuspended in 40 mL lysis buffer
578 (20 mM Tris-Cl pH = 7.5, 300 mM NaCl, 10 mM imidazole pH = 7.0, 1 mM DTT, protease
579 inhibitor cocktail). Resuspended cells were disrupted with a microfluidizer and the cell debris
580 was removed at 20,000 x *g* for 30 minutes at 4 °C. The Nb^{traN}/$TraN^{surf}$ protein complex was
581 then purified from the supernatant individually by gravity flow through a 2 mL Ni-NTA agarose
582 column. Bound proteins were then eluted using a linear imidazole gradient to a final
583 concentration of 300 mM. The purity of each protein sample was assessed by 15% SDS-PAGE
584 followed by Coomassie Brilliant Blue staining. Protein samples were further purified by fast
585 protein liquid chromatography (FPLC) using gel filtration on a HiLoad 16/600 Superdex 200pg
586 column (**Supplementary Fig. 3b**).
587 For protein binding experiments requiring free $TraN^{surf}$ and nanobodies, proteins were
588 overproduced in *E. coli* strain BL21 (DE3) pRIL transformed with the IPTG expression vectors
589 containing the desired genes. Cultures were grown in LB medium at 37 °C to log phase (OD_{600}
590 = 0.6~0.8) and induced by IPTG. After induction at 30 °C, the cells were precipitated and
591 resuspended in lysis buffer as described above. Resuspended cells were disrupted using a
592 microfluidizer. The cellular debris was removed by centrifugation at 20,000 x *g* for 30 minutes

593 at 4 °C. The histidine-tagged proteins were purified from the supernatant by gravity flow
594 through a 2 ml Ni-NTA agarose column. Bound proteins were then eluted using a linear
595 imidazole gradient to a final concentration of 300 mM. All protein samples were further
596 purified by FPLC using gel filtration on a HiLoad 16/600 Superdex 200pg column. Fractions
597 with high purity were concentrated and used in binding assays.
598
599 **Crystallization and Structure Determination**
600 For crystallization of the $Nb^{traN}/TraN^{surf}$ complex, the Ni-NTA-purified protein was
601 dialyzed in low salt buffer (5 mM Tris-HCl pH = 7.0, 150 mM NaCl, 0.5 mM TCEP) and
602 concentrated to ~20 mg/mL by spin filtration (10 kDa cutoff, Millipore). The concentrated
603 sample was subsequently screened against commercially available crystallization screens from
604 Hampton Research. Diffraction-quality crystals were successfully generated at 20 °C via
605 hanging drop vapor diffusion in three weeks, maintaining a buffer-to-protein ratio of 1:2. The
606 crystallization solution, conducive to crystal formation, consisted of 1 M ammonium sulfate
607 and 0.1 M sodium acetate at pH = 4.6.
608 Cryo-protection of $Nb^{traN}/TraN^{surf}$ complex crystals was performed in 20% (*v/v*)
609 glycerol in the crystallization solution described above. The X-ray diffraction datasets were
610 collected on beamline TPS-07A at the National Synchrotron Radiation Research Center
611 (Taiwan). X-ray diffraction intensities were processed using HKL 2000[42]. Phase determination
612 of the $Nb^{traN}/TraN^{surf}$ complex was carried out using molecular replacement by Phaser in
613 PHENIX, with poly-alanine nanobody (PDB: 5VNV) as a search model[43]. The $Nb^{traN}/TraN^{surf}$
614 complex model was built into the electron density map and further refined by Coot and
615 PHENIX, respectively[43, 44]. Crystals were cubic (space group P212121), with five complexes
616 per asymmetric unit. There are no residues in the unfavored region of the Ramachandran plots.
617 Data collection and refinement statistics are shown in **Supplementary Table 1**.
618
619 **Fluorescence Microscopy**
620 Bacterial cultures were grown overnight in M9 minimal medium at 37 °C with 200 rpm
621 shaking. The cells were harvested by centrifugation at 8,000 x *g* for 1 minute. The culture
622 supernatant was removed and washed with Phosphate-buffered saline (PBS) by spinning at
623 8,000 x *g* for 1 minute. The washed cells were resuspended in PBS containing 1%
624 paraformaldehyde (PFA) for 1-hour cell fixation at room temperature. The fixed cells were
625 subjected to three PBS washes. The cell suspensions were then adjusted to OD_{600} = 1.0 using
626 PBS. The addition of 2 μM of Nb-GFPs to the cell suspensions preceded a 1-hour incubation

627 at 37 °C with shaking at 200 rpm for nanobody binding. The cells were then washed four times
628 with PBS at 6,000 x *g* for 1 minute. Cell suspensions were spotted on a 1.5% agarose pad
629 settled on a microscope slide. Images were captured using a DeltaVision Core Deconvolution
630 Microscopy system with an Olympus IX71 microscope and a 60x 1.42 NA oil-immersion
631 objective.
632
633 **Determination of Nanobody Library Genetic Diversity**
634 To analyze the diversity of the nanobody population within each round of the selection
635 process, cells were harvested and total plasmids were extracted for targeted amplicon
636 sequencing[45]. Nanobody genes were amplified through 20 cycles of PCR using specific primers
637 (**Supplementary Table 2**). Eight unique molecular identifiers (UMI) were incorporated before
638 the 5' primers to eliminate duplicate molecules resulting from PCR amplification. The PCR
639 amplicons with a gel size of around 400 bp were selected and extracted using a QIAquick Gel
640 Extraction Kit. The purified amplicons were then quantified using Qubit DNA HS reagent, and
641 the 400 bp size amplicons were verified using a Bioanalyzer 2100 system (Agilent
642 Technologies).
643 Next, Index 1 (i7) and Index 2 (i5) sequences were added to the cleanup samples to
644 generate uniquely tagged libraries by employing the Illumina DNA/RNA UD Indexes Set B,
645 followed by eight cycles of PCR using the Index primers and KAPA HiFi HotStart Ready Mix.
646 The indexed amplicons were subsequently cleaned up by Ampure XP reagent and quantified.
647 The final library was quantified to confirm the expected size of around 489 bp, and the
648 concentration was calculated using an Illumina pooling calculator. The library samples were
649 then diluted to 2 nM and submitted for Illumina MiSeq sequencing, which was performed by
650 the Genomics Core of the Institute of Molecular Biology (Academia Sinica, Taiwan).
651 Raw data analysis was conducted as follows. Initially, nanobody sequences were
652 identified through the 5' and 3' primers, as detailed in **Supplementary Table 2**. Reads with the
653 same UMI sequences were considered to have originated from the same original molecule,
654 enabling the removal of duplicate reads that arise during library amplification steps and
655 ensuring more accurate quantification of the diversity and abundance of unique molecules in
656 the samples. The variable region was subsequently determined by scrutinizing the 25-bp
657 segments upstream and downstream of conserved sequences. Alignment of each conserved
658 sequence with the nanobody was achieved using the Smith-Waterman algorithm for local
659 sequence alignment[46]. The variable region was delineated based on the alignments of conserved
660 sequences at both ends. In cases where the number of mismatches exceeded five, the variable

661 region was deemed absent. Lastly, all variable regions underwent clustering, and their
662 frequencies were tallied (**Supplementary Table 3**).
663
664 **Conjugative Scores Measurement**
665 To analyze the deep mutational scanning data, log2 enrichment ratios of mutations (*Mut*)
666 were normalized by subtracting the enrichment ratios of the wild-type (*Wt*) sequence according
667 to the following formula (**Supplementary Fig. 5a and Supplementary Table 3**):
668
669 $$Conjugative\ score = log_2\left[\frac{Mut_{P1}(\%)}{Mut_{P0}(\%)}\right] - log_2\left[\frac{Wt_{P1}(\%)}{Wt_{P0}(\%)}\right]$$
670
671 **Target Cell Depletion Assay**
672 The target cell depletion assays were carried out as described previously[8]. In brief,
673 overnight PIC cultures were diluted to OD_{600} = 0.05 and grown at 37 °C for 4 hours in LB broth
674 with aTc to induce surface-exposed nanobodies (Nb^{ompA}, Nb^{ompC}, or Nb^{BamA}). The cells were
675 then pelleted, washed, and resuspended in LB, and then normalized to OD_{600} = 2. Mixtures of
676 PICs and the indicated *E. coli* strains were then established at a 100:1 *v/v* ratio in LB broth with
677 aTc. Bacterial mixtures were incubated at 37 °C with shaking at 200 rpm, and samples were
678 collected at 0, 30, 60, and 90 minutes, followed by serial dilution and plating on selective media
679 to quantify CFUs. PICs were distinguished by plating on LB containing streptomycin (intrinsic
680 resistance), whereas *E. coli* were plated on LB containing chloramphenicol (chromosomal
681 insertion of the chloramphenicol acetyltransferase gene).
682 For target depletion experiments in undefined bacterial communities, three reared
683 C57BL/6J mice were fed by 200 µL oral gavage in 20% (*w/v*) sucrose solution containing 10^9
684 CFUs of log-phase wild-type *E. coli* MG1655. Following ingestion of the bacterial suspension,
685 the mice were provided with both standard rodent food and sterilized water. Fecal samples were
686 collected at 24 hours post-feeding and suspended in 6 mL of PBS, and then homogenized using
687 a tissue-tearor with a probe diameter of 7 mm (BioSpec). The samples were then gently added
688 to the top of 2 mL of 80% (*w/v*) Nycodenz, followed by ultra-centrifugation at 10,000 x *g* for
689 40 minutes. The top layer of PBS solution was carefully removed, and the high-density fecal
690 bacterial community from the middle layer was collected and normalized to OD_{600} = 3 in PBS.
691 The resulting fecal bacterial community was mixed with an equal volume of PICs (OD_{600} =
692 2.0) expressing Nb^{ompA}, Nb^{ompC}, or Nb^{BamA} as described above. The bacterial mixtures were
693 incubated at 37 °C with shaking at 200 rpm for 1 hour. Pre- and post-incubation samples were

694 plated on LB with chloramphenicol or streptomycin to selectively quantify *E. coli* or PIC
695 populations, respectively.
696
697 **Analysis of Protein Expression Levels**
698 To analyze the expression level of nanobodies, *E. coli* expressing Nb^{traN} (wild-type and
699 variants) were grown in LB medium supplemented with or without aTc at 37 °C for 6 hours
700 and harvested at an OD_{600} of 1.0. For each quantification assay, cell pellets were resuspended
701 in SDS-PAGE sample loading buffer. Samples were boiled at 100 °C for 10 minutes and equal
702 volumes were loaded for SDS-PAGE, before being transferred to nitrocellulose membranes.
703 Membranes were blocked in TBST (10 mM Tris-HCl pH 7.5, 150 mM NaCl, 0.1% (*w/v*)
704 Tween-20) with 5% (*w/v*) non-fat milk for 30 minutes at room temperature, followed by
705 incubation for 1 hour at room temperature with primary antibodies (anti-c-myc or anti-RNA
706 Polymerase β) diluted 1:1000 in TBST. Blots were then washed by TBST, followed by
707 incubation for 30 minutes at room temperature with the secondary antibody (anti-mouse IgG
708 HRP conjugated) diluted 1:5000 in TBST. Finally, blots were washed again by TBST,
709 developed, and visualized using a UVP Biospectrum 815 system.
710
711 **Isothermal Titration Calorimetry (ITC)**
712 Titration experiments were performed using a Microcal PEAQ-ITC automated system
713 (Malvern) at 25 °C. The ITC sample cell contained 390μL of 40μM $TraN^{surf}$ in Tris buffer (20
714 mM Tris-Cl pH = 7.5, 150 mM NaCl, 0.5 mM TCEP). A syringe containing 125 μL of 500 μM
715 Nb^{traN} or nanobody variants (Nb^{traN}_F47A/Y58A, Nb^{traN}_Y98A/L100A, Nb^{traN}_S105C, and
716 Nb^{traN}_H106C) in the same Tris buffer was used to inject into the sample cell using 20x
717 injections. The raw experimental data were analyzed using the MicroCal PEAQ-ITC Analysis
718 software package provided with the instrument. The fitting function in the software was
719 generated by clicking the iteration button until an excellent fit to the experimental data points
720 of the isotherms had been obtained. The final parameters, including K_D, changes in enthalpy
721 (ΔH), Gibb's free energy (ΔG), and entropy (ΔS), were generated by the same software.
722
723 **Quantification and Statistical Analyses**
724 Statistical significance in bacterial competition experiments was assessed by unpaired
725 t-tests between relevant samples. Details of statistical significance are provided in the figure
726 legends.
727

ACKNOWLEDGMENTS

We thank Drs. Marcos de Moraes, Yu-Chan Chao, and Ting laboratory members for helpful discussions and critical reading of the manuscript; Drs. Joseph Moguous, Yun Mou, Shu-Jung Chang, Hsin-Hung Chou, Liuh-Yow Chen, Jen-Hsuan Wei, Jun-Yi Leu, and Sue Lin-Chao for sharing reagents; Dr. Soo-Chen Cheng for sharing equipment; Drs. Shu-Yun Tung, Hsin-Nan Lin, Chen-Hsin Yu, Ching-Hung Tseng, and Xin-Jie Huang for technical assistance; and Dr. John O'Brien for manuscript editing. We acknowledge funding support from Academia Sinica (AS-CDA-112-L05 to S.-Y.T., AS-IVA-112-L05 to K.-C.H.) and the National Science and Technology Council, Taiwan (111-2311-B-001-006-MY2 and 112-2311-B-001-020 to S.-Y.T., 112-2320-B001-005-MY2 to W.-L.W., 112-2320-B-001-006-MY3 to K.-C.H.).

FIGURE LEGENDS

Fig. 1. Establishment of the whole-cell-based CAM discovery platform in liquid medium. (**a**) Schematic of the strategy for facilitating precise DNA conjugation between specific cells through synthetic cell-cell adhesion. Bacteria expressing diverse nanobodies (Nb) and conjugative cells with surface antigens (Ag) are involved. (**b**) The whole-cell-based selection platform is designed to identify nanobody CAMs targeting specific antigens of interest. Conjugative cells expressing the target antigen and cells displaying the nanobody library are employed. ① Within a liquid culture, contact-dependent DNA conjugation is enhanced through strong binding between cognate nanobodies and antigen pairs (both labeled in blue). ② After conjugation, antibiotics are used to eliminate conjugative cells and recipients expressing non-nanobody binders. ③ After a single round of selection, transconjugants carrying nanobodies with a relatively strong binding affinity toward the target antigens are enriched. (**c**) Conjugation frequencies (transconjugants/total recipients) of conjugative plasmids (pGenR, pAmpR, and pTmpR) were assessed under both solid and liquid growth conditions for a 6-hour duration. *E. coli* S17-1 serves as the conjugative donor strain, and MG1655 serves as the recipient strain. (**d**) Conjugation frequency of pGenR under the liquid growth condition. Recipient cells expressing nanobodies were co-cultured with donor cells displaying cognate or orthogonal antigens. Data are presented as means ± SD. n = 3 technical replicates, representative of two biological replicates. *$p < 0.05$, t-test. See also **Supplementary Fig. 1**.

Fig. 2. Iterative rounds of bio-panning enhance the discriminant capacity of the CAM selection platform.
(**a**) Conjugation frequency of pGenR in conjugation assays within liquid culture between recipient and donor displaying Ag1 or Control (without antigen displayed). The recipient culture expressing Nb1 was 10-, 100-, 1000-, and 10000-fold diluted with the culture expressing non-matched null cells. (**b**) Schematic of three-round selection. For each round, donors (yellow) carry plasmids containing antibiotic-resistance genes against gentamicin (GenR), ampicillin (AmpR), or trimethoprim (TmpR) as distinct selection markers. The cartoon illustration on the right represents the progressive increase in the abundance of recipient cells displaying Nb1 (blue) in a mixed population with non-matched null cells (grey) during the selection process. (**c**) Conjugation frequency in two rounds of bio-panning. The initial population of recipient cells expressing Nb1 and null cells were mixed at a ratio of $1:10^5$.

(**d**) Conjugation frequency in three rounds of bio-panning. The initial population of recipient cells expressing Nb1 and null cells were mixed at a ratio of $1:10^7$. Data are presented as means ± SD. n ≥ 3 technical replicates, representative of two biological replicates. *$p < 0.05$, t-test. See also **Supplementary Fig. 2**.

Fig. 3. Identification of nanobody recognizing TraN via the CAM discovery platform. (**a**) Stacked bar plot illustrating the changes in the relative abundance of individual nanobodies within the population across three rounds of bio-panning to enrich for bacteria displaying TraN-binding nanobodies. Sequences were discerned through the CDR regions of the nanobody gene. The relative abundances of all unique nanobodies identified are shown, and the respective counts are detailed in **Supplementary Table 3**. Colors denote the ranking of nanobody abundance from the highest to lowest. (**b**) Macroscopic aggregation analysis to assess cell-cell adhesion. Cultures of *E. coli* strains displaying TraN or Nb^{traN} were incubated either individually or in combination. The OD_{600} of the supernatant after the settling period is shown below the image. (**c**) The amino acid sequence of Nb^{traN}, shows CDR1, CDR2, and CDR3 in green, blue, and orange, respectively. (**d, e**) The ITC binding profiles of Nb^{traN} with $TraN^{surf}$ at 25 °C. (**f**) Crystal structure of Nb^{traN} (yellow) in complex with $TraN^{surf}$ (blue) (PDB: 8X7N). CDR1, CDR2, and CDR3 are presented in green, blue, and orange, respectively. (**g**) A magnified view of the interacting residues is indicated between Nb^{traN} and $TraN^{surf}$. See also **Supplementary Table 1**.

Fig. 4. Discovery of optimized Nb^{traN} variants through deep mutational scanning (**a**) Selection workflow of the deep mutational scanning. Plasmids carrying Nb^{traN} genes with single-site mutations in CDR3 were utilized for library construction. The mutant library underwent a single round of selection with donor cells displaying TraN to enrich for bacteria expressing potent Nb^{traN} variants displaying stronger binding capacity. (**b**) The conjugative scores of individual Nb^{traN} CDR3 mutations are depicted in a heatmap. The X-axis represents individual amino acid mutation, and the Y-axis represents the residue position of CDR3 in wild-type Nb^{traN}. Mutations not identified after selection were excluded from the analysis and are shown in black (N/A). (**c**) Macroscopic aggregation analysis to assess cell-cell adhesion between *E. coli* strains displaying TraN and the indicated Nb^{traN} variants. The OD_{600} of the culture supernatant is shown below the image. The cells expressing TraN or wild-type Nb^{traN} were used as controls. (**d**) Immunoblotting analysis of *E. coli* expressing the Nb^{traN} variants carrying a C-terminal myc tag after a 16-hour incubation. The loading control is *E. coli* RNA Polymerase β protein (RpoB). Migrations of a size standard, in kDa, are indicted (left). (**e**) Conjugation frequency of pGenR under the liquid growth condition. Recipient cells expressing indicated nanobodies were co-cultured with donor cells expressing TraN. Data are presented as means ± SD. n = 3 technical replicates, representative of two biological replicates. *$p < 0.05$, t-test. (**f, g**) The ITC binding profiles of the indicated Nb^{traN} variants with $TraN^{surf}$ at 25 °C. See also **Supplementary Fig. 5 and 6**.

Fig. 5. Nanobody CAM targeting of *E. coli* integral membrane proteins OmpA and OmpC. (**a**) The amino acid sequence of Nb^{ompA} and Nb^{ompC}. CDR1 (green), CDR2 (red), and CDR3 (blue) are indicated. (**b**) Self-aggregation of *E. coli* expressing Nb^{ompA} and Nb^{ompC}. Cultures underwent 24-hour aTc induction before settling. Cultures that did not undergo induction (*i.e.,* not expressing nanobodies) are presented as controls. (**c, d**) Conjugation frequency of pGenR under the liquid growth condition. Recipient cells expressing indicated nanobodies were co-cultured with S17-1 donor cells expressing (**c**) or not expressing (**d**) the indicated antigens. Data are presented as means ± SD. n = 3 technical replicates, representative of two biological replicates. *$p < 0.05$, t-test. (**e, f**) Fluorescence micrographs showing the antigen-binding

822 specificity of Nb^{ompA}-GFP (**e**) and Nb^{ompC}-GFP (**f**). Nb^{ompA}-GFP and Nb^{ompC}-GFP were
823 incubated with wild-type *E. coli* and the antigen-deleted strains (Δ*ompA* or Δ*ompC*) for 1 hour
824 before observation. Scale bar = 1 μm. Full-size images are available in **Supplementary Fig. 8**.
825
826 **Fig. 6. Mounting Nb^{ompA} and Nb^{ompC} on PICs depletes target *E. coli* from bacterial**
827 **mixtures.**
828 (**a**) Schematic of target depletion of bacteria (green) from a complex bacterial population by
829 PICs (pink). (**b-e**) Survival (CFUs/mL) of *E. coli* strains (wild-type, Δ*ompA*, Δ*ompC*, and
830 Δ*rfaD*, colored green, yellow, blue, and orange, respectively) upon incubation with PICs
831 displaying Nb^{ompA} (**b**), Nb^{ompC} (**c**), non-match control (Ctrl) (**d**), or Nb^{BamA} (**e**) in liquid medium
832 (n = 3 technical replicates ± S.D.; *$p < 0.05$, t-test). Two biological repeats were conducted. (**f**)
833 Survival (CFUs/mL) of wild-type *E. coli* within a mouse fecal bacterial population before and
834 after incubation with PICs displaying Nb^{ompA}, Nb^{ompC}, or Nb^{BamA} (n = 3 technical replicates ±
835 S.D., representative of two biological replicates. *$p < 0.05$, t-test). See also **Supplementary**
836 **Fig. 9 and 10**.
837
838 # SUPPLEMENTAL FIGURE LEGENDS
839
840 **Fig. S1. Dependency of selection marker gene transfer on a functional T4SS.**
841 (**a**) The conjugation frequency of selection markers from the WT and Δ*trbE* (dysfunctional
842 T4SS) donors to recipients. Conjugation assays were performed under both liquid and solid
843 growth conditions, utilizing pGenR, pCarbR, and pTmpR as selection markers. (**b**) The impact
844 of a deficient T4SS on the donor (*E. coli* S17-1) to convey the selection marker (pGenR) to the
845 recipient (*E. coli* MG1655). Two binding pairs were employed: Ag1 and AgInt were displayed
846 by the donors, and their corresponding nanobodies (Nb1 and NbIB10) were displayed by the
847 recipients. Data are presented as means ± SD. n = 3 technical replicates, representative of two
848 biological replicates. *$p < 0.05$, t-test. Conjugation frequency lower than the detection limit
849 designated as N/A.
850
851 **Fig. S2. Diagnostic PCR verification of the efficacy of the selection strategy in enriching**
852 **for low-abundance nanobodies.**
853 (**a**) The display system employed in this study comprises the intimin N-terminus (grey) fused
854 with the adhesin region (yellow) at the C-terminus. Arrows indicate the annealing primers
855 utilized for diagnostic PCR. The expected length of the PCR products for the cells displaying
856 Nb1 (640 bp) and null (261 bp) are underscored. (**b**) PCR analysis of the transconjugants after
857 selection. Two recipient strains expressing Nb1 and non-matched null control, respectively,
858 were mixed at an initial ratio of $1:10^3$. The primers illustrated in (**a**) were used for diagnostic
859 PCR. The proportions of colonies expressing Nb1 are denoted at the bottom-right (red). (**c**)
860 Randomly selected colonies after two rounds of bio-panning were subjected to diagnostic PCR.
861 The recipient cells displaying Nb1 were diluted with cells expressing a non-matched null
862 control at an initial ratio of $1:10^5$. (**d**) The recipient population, initially at a ratio of Nb1:Null
863 = $1:10^7$, after three rounds of selection was verified through diagnostic PCR.
864
865 **Fig. S3. Nb^{traN} binds to TraN.**
866 (**a**) The macroscopic aggregation analysis to assess cell-cell adhesion for the indicated cultures
867 of *E. coli* strains either individually or in combination. *E. coli* displaying TraN, Nb^{traN}, or the
868 non-matched control (Ctrl) were tested. The OD_{600} of the culture supernatants was measured
869 after the settling period. (**b**) Size-exclusion chromatography profile of the Nb^{TraN}/$TraN^{surf}$
870 complex using a HiLoad 16/600 Superdex 200pg column. (**c**) The coomassie-stained SDS-
871 PAGE protein gel shows the elution fractions of Nb^{traN} in complex with $TraN^{surf}$. Migrations of

a size standard, in kDa, are indicted (left).

Fig. S4. Mutations in the CDR2 or CDR3 of Nb^{traN} affect its interaction with TraN.
(**a**) Comparison of the adhesive capability of the wild-type (wt) Nb^{traN} and its variants (CDR2: F47A/Y58A; CDR3: Y98A/L101A). For the macroscopic aggregation analysis, single cultures and mixtures were used. After settling, the OD_{600} of the culture supernatants was measured and values are shown below the image. (**b, c**) The ITC binding profiles of Nb^{traN} F47A/Y58A with $TraN^{surf}$. (**d, e**) The ITC binding profiles of Nb^{traN} Y98A/L101A with $TraN^{surf}$.

Fig. S5. Deep mutational engineering of CDR3 in Nb^{traN}.
(**a**) The values of the conjugative scores of single amino acid substitution within CDR3 of Nb^{traN}. Related to **Fig. 4**. (**b**) Crystal Structure of Nb^{traN} (yellow) bound to the surface-exposed domain of TraN ($TraN^{surf}$, blue) (PDB: 8X7N). A second view (rotated 180° around the vertical axis) is shown below. The close-up views on the right side indicate the locations of the cysteine variants (residues 101 to 107) on Nb^{traN}.

Fig. S6. Residue substitutions of CDR3 in Nb^{traN} improve its binding to TraN.
(**a**) Control cultures of *E. coli* strains expressing the Nb^{traN} variants that were used in the macroscopic aggregation assay in **Fig. 4**. (**b, c**) The ITC binding profiles of Nb^{traN} S105C (**b**) and H106C (**c**) with $TraN^{surf}$. Related to **Fig. 4**.

Fig. S7. Structures of *E. coli* OmpA and OmpC.
Crystal structures of the OmpA membrane domain (PBD: 1QJP)[1] and OmpC (PDB: 2J1N)[2] from *E. coli*. OmpA (blue) is presented as a monomeric structure, featuring an eight-stranded β-barrel spanning the outer membrane, coupled with flexible loops at its external end. Homotrimeric OmpC (green) is composed of three beta-barrels. The monomeric form of OmpC exhibits a 16-stranded β-barrel porin fold, with irregular extracellular loops.

Fig. S8. Nb^{ompA}-GFP and Nb^{ompC}-GFP bind to their target antigens.
(**a**) The phase-contrast (top), green fluorescence (middle), and merged (bottom) images of *E. coli* (wild-type and *ΔompA* strain) following 1-hour incubation with Nb^{ompA}-GFP. The white borders demarcate the cropped images displayed in **Fig. 5e**. (**b**) Fluorescence micrographs of *E. coli* (wild-type and *ΔompC* strain) cells treated with Nb^{ompC}-GFP for 1 hour. Phase-contrast (top), green fluorescence (middle), and merged (bottom) images are presented. Zoomed-in images of the areas within white borders are featured in **Fig. 5f**.

Fig. S9. Target depletion mediated by PICs requires a functional T6SS, and survival of PICs upon incubation with target *E. coli*.
(**a, c, e, g**) Survival (CFUs/mL) of *E. coli* MG1655 wild-type, Δ*ompA*, Δ*ompC*, and Δ*rfaD* strains (colored green, yellow, blue, and orange, respectively) upon liquid co-culture with T6SS-deficient PICs expressing Nb^{ompA} (**a**), Nb^{ompC} (**c**), non-matched control (**e**), or Nb^{BamA} (**g**). (**b, d, f, h**) The survival CFU of PICs expressing Nb^{ompA} (**b**), Nb^{ompC} (**d**), non-matching control (**f**), or Nb^{BamA} (**h**) upon liquid co-culture with target cells *E. coli* MG1655 wild-type (green), Δ*ompA* (yellow), Δ*ompC* (blue), and Δ*rfaD* (orange) cells. PICs with a functional (T6SS+) or dysfunctional T6SS (T6SS−, Δ*icmF*) were utilized. Data are presented as means ± SD. n = 3 technical replicates, representative of two biological replicates. *$p < 0.05$, t-test.

Fig. S10. Survival of PICs remains unaffected before and after incubation in a bacterial mixture derived from mice fecal samples.

(a) Phase-contrast micrograph of a bacterial population isolated from mouse fecal samples. Scale bar = 5 μm. (**b**) Survival (CFUs/mL) of PICs before and after incubation with mouse fecal microbiota. Related to **Fig. 6f**.

Supplementary Table 1

X-ray data collection and refinement statistics. Relevant to Method and **Fig. 3**.

Supplementary Table 2

Strains, Recombinant DNA, and Oligonucleotides used in this study.

Supplementary Table 3

Illumina MiSeq deep-sequencing analysis of the nanobodies against TraN antigen. Related to **Fig. 3 and 4**.

DATA AVAILABILITY

The coordinates and structure factors for the $Nb^{traN}/TraN^{surf}$ complex have been deposited in the Protein Data Bank, with accession code 8X7N. Sequence data associated with this study is available from the Sequence Read Archive at GSE249103.

AUTHOR CONTRIBUTIONS

P.-Y.C., W.-L.W., K.-C.H., and S.-Y.T. designed the study. P.-Y.C., Y.-C.C., P.-P.C., K.-T.L., and K.-C.H. performed experiments. P.-Y.C., Y.-C.C., P.-P.C., K.-C.H., and S.-Y.T. analyzed data. P.-Y.C., Y.-C.C., P.-P.C., K.-C.H., and S.-Y.T. wrote the manuscript.

REFERENCES

1. Pautsch, A. & Schulz, G.E. High-resolution structure of the OmpA membrane domain. *J Mol Biol* **298**, 273-282 (2000).
2. Basle, A., Rummel, G., Storici, P., Rosenbusch, J.P. & Schirmer, T. Crystal structure of osmoporin OmpC from E. coli at 2.0 A. *J Mol Biol* **362**, 933-942 (2006).
3. Kim, H. *et al.* 4-bit adhesion logic enables universal multicellular interface patterning. *Nature* **608**, 324-329 (2022).
4. Xavier, J.B. Social interaction in synthetic and natural microbial communities. *Mol Syst Biol* **7**, 483 (2011).
5. Chen, B. *et al.* Programmable living assembly of materials by bacterial adhesion. *Nat Chem Biol* **18**, 289-294 (2022).
6. Nadell, C.D., Drescher, K. & Foster, K.R. Spatial structure, cooperation and competition in biofilms. *Nat Rev Microbiol* **14**, 589-600 (2016).
7. Chen, H.J., Peng, C.F., Tang, C.W. & Chen, Y.T. Self-Healing Concrete by Biological Substrate. *Materials (Basel)* **12** (2019).
8. Ting, S.Y. *et al.* Targeted Depletion of Bacteria from Mixed Populations by Programmable Adhesion with Antagonistic Competitor Cells. *Cell Host Microbe* **28**, 313-321 e316 (2020).

961 9. Robledo, M. *et al.* Targeted bacterial conjugation mediated by synthetic cell-to-cell
962 adhesions. *Nucleic Acids Res* **50**, 12938-12950 (2022).
963 10. Li, Y.G., Kishida, K., Ogawa-Kishida, N. & Christie, P.J. Ligand-displaying Escherichia coli
964 cells and minicells for programmable delivery of toxic payloads via type IV secretion
965 systems. *mBio*, e0214323 (2023).
966 11. Glass, D.S. & Riedel-Kruse, I.H. A Synthetic Bacterial Cell-Cell Adhesion Toolbox for
967 Programming Multicellular Morphologies and Patterns. *Cell* **174**, 649-658 e616 (2018).
968 12. Chao, G. *et al.* helixCAM: A platform for programmable cellular assembly in bacteria
969 and human cells. *Cell* **185**, 3551-3567 e3539 (2022).
970 13. Krohl, P.J. *et al.* Discovery of antibodies targeting multipass transmembrane proteins
971 using a suspension cell-based evolutionary approach. *Cell Rep Methods* **3**, 100429
972 (2023).
973 14. Stark, Y., Venet, S. & Schmid, A. Whole Cell Panning with Phage Display. *Methods Mol*
974 *Biol* **1575**, 67-91 (2017).
975 15. Klimke, W.A. *et al.* The mating pair stabilization protein, TraN, of the F plasmid is an
976 outer-membrane protein with two regions that are important for its function in
977 conjugation. *Microbiology (Reading)* **151**, 3527-3540 (2005).
978 16. Salema, V. *et al.* Selection of single domain antibodies from immune libraries displayed
979 on the surface of E. coli cells with two beta-domains of opposite topologies. *PLoS One*
980 **8**, e75126 (2013).
981 17. Ferrieres, L. *et al.* Silent mischief: bacteriophage Mu insertions contaminate products
982 of Escherichia coli random mutagenesis performed using suicidal transposon delivery
983 plasmids mobilized by broad-host-range RP4 conjugative machinery. *J Bacteriol* **192**,
984 6418-6427 (2010).
985 18. del Campo, I. *et al.* Determination of conjugation rates on solid surfaces. *Plasmid* **67**,
986 174-182 (2012).
987 19. Haase, J., Lurz, R., Grahn, A.M., Bamford, D.H. & Lanka, E. Bacterial conjugation
988 mediated by plasmid RP4: RSF1010 mobilization, donor-specific phage propagation,
989 and pilus production require the same Tra2 core components of a proposed DNA
990 transport complex. *J Bacteriol* **177**, 4779-4791 (1995).
991 20. Ruano-Gallego, D., Fraile, S., Gutierrez, C. & Fernandez, L.A. Screening and purification
992 of nanobodies from E. coli culture supernatants using the hemolysin secretion system.
993 *Microb Cell Fact* **18**, 47 (2019).
994 21. Low, W.W. *et al.* Mating pair stabilization mediates bacterial conjugation species
995 specificity. *Nat Microbiol* **7**, 1016-1027 (2022).
996 22. McMahon, C. *et al.* Yeast surface display platform for rapid discovery of
997 conformationally selective nanobodies. *Nat Struct Mol Biol* **25**, 289-296 (2018).
998 23. Zavrtanik, U., Lukan, J., Loris, R., Lah, J. & Hadzi, S. Structural Basis of Epitope
999 Recognition by Heavy-Chain Camelid Antibodies. *J Mol Biol* **430**, 4369-4386 (2018).
1000 24. Samsudin, F., Ortiz-Suarez, M.L., Piggot, T.J., Bond, P.J. & Khalid, S. OmpA: A Flexible
1001 Clamp for Bacterial Cell Wall Attachment. *Structure* **24**, 2227-2235 (2016).
1002 25. Nikaido, H. Molecular basis of bacterial outer membrane permeability revisited.
1003 *Microbiol Mol Biol Rev* **67**, 593-656 (2003).
1004 26. Russell, A.B. *et al.* Diverse type VI secretion phospholipases are functionally plastic
1005 antibacterial effectors. *Nature* **496**, 508-512 (2013).
1006 27. Whitney, J.C. *et al.* Genetically distinct pathways guide effector export through the type
1007 VI secretion system. *Mol Microbiol* **92**, 529-542 (2014).

28. Kaur, H. *et al.* Identification of conformation-selective nanobodies against the membrane protein insertase BamA by an integrated structural biology approach. *J Biomol NMR* **73**, 375-384 (2019).
29. Grohmann, E., Christie, P.J., Waksman, G. & Backert, S. Type IV secretion in Gram-negative and Gram-positive bacteria. *Mol Microbiol* **107**, 455-471 (2018).
30. Rathinam, N.K. & Sani, R.K. in ACS symposium series 1329 1 online resource (American Chemical Society,, Washington, DC; 2019).
31. Lam, K.N. *et al.* Phage-delivered CRISPR-Cas9 for strain-specific depletion and genomic deletions in the gut microbiome. *Cell Rep* **37**, 109930 (2021).
32. Jin, W.B. *et al.* Genetic manipulation of gut microbes enables single-gene interrogation in a complex microbiome. *Cell* **185**, 547-562 e522 (2022).
33. Lopez-Igual, R., Bernal-Bayard, J., Rodriguez-Paton, A., Ghigo, J.M. & Mazel, D. Engineered toxin-intein antimicrobials can selectively target and kill antibiotic-resistant bacteria in mixed populations. *Nat Biotechnol* **37**, 755-760 (2019).
34. Kunkel, T.A. Rapid and efficient site-specific mutagenesis without phenotypic selection. *Proc Natl Acad Sci U S A* **82**, 488-492 (1985).
35. Gibson, D.G. *et al.* Enzymatic assembly of DNA molecules up to several hundred kilobases. *Nat Methods* **6**, 343-345 (2009).
36. Edwards, R.A., Keller, L.H. & Schifferli, D.M. Improved allelic exchange vectors and their use to analyze 987P fimbria gene expression. *Gene* **207**, 149-157 (1998).
37. Lee, P.C., Stopford, C.M., Svenson, A.G. & Rietsch, A. Control of effector export by the Pseudomonas aeruginosa type III secretion proteins PcrG and PcrV. *Mol Microbiol* **75**, 924-941 (2010).
38. Cardona, S.T. & Valvano, M.A. An expression vector containing a rhamnose-inducible promoter provides tightly regulated gene expression in Burkholderia cenocepacia. *Plasmid* **54**, 219-228 (2005).
39. Choi, K.H. *et al.* A Tn7-based broad-range bacterial cloning and expression system. *Nat Methods* **2**, 443-448 (2005).
40. Datsenko, K.A. & Wanner, B.L. One-step inactivation of chromosomal genes in Escherichia coli K-12 using PCR products. *Proc Natl Acad Sci U S A* **97**, 6640-6645 (2000).
41. Low, W.W., Seddon, C., Beis, K. & Frankel, G. The Interaction of the F-Like Plasmid-Encoded TraN Isoforms with Their Cognate Outer Membrane Receptors. *J Bacteriol* **205**, e0006123 (2023).
42. Otwinowski, Z. & Minor, W. Processing of X-ray diffraction data collected in oscillation mode. *Methods Enzymol* **276**, 307-326 (1997).
43. Adams, P.D. *et al.* PHENIX: a comprehensive Python-based system for macromolecular structure solution. *Acta Crystallogr D Biol Crystallogr* **66**, 213-221 (2010).
44. Emsley, P. & Cowtan, K. Coot: model-building tools for molecular graphics. *Acta Crystallogr D Biol Crystallogr* **60**, 2126-2132 (2004).
45. Naik, T., Sharda, M., C, P.L., Virbhadra, K. & Pandit, A. High-quality single amplicon sequencing method for illumina MiSeq platform using pool of 'N' (0-10) spacer-linked target specific primers without PhiX spike-in. *BMC Genomics* **24**, 141 (2023).
46. Smith, T.F. & Waterman, M.S. Identification of common molecular subsequences. *J Mol Biol* **147**, 195-197 (1981).

1054 **Supplementary Table 1. X-ray data collection and refinement statistics.**
1055

Crystals	$TraN^{surf}/Nb^{traN}$ complex
Space group	$2_1\ 2_1\ 2_1$
Cell dimensions	
a, b, c (Å)	a= 96.864 b=153.263 c=163.03
α, β, γ (o)	α=β=γ=90
Data collection	
Wavelength (Å)	0.97625
Resolution	19.85 -3.67
Total reflections	230515
Unique reflections	26580
R_{merge} (%)[a]	20.5 (63.9)
CC1/2 (%)[a]	98.8 (95.5)
$I / \sigma I$ [a]	7.3 (2.6)
Completeness (%)	99.8 (98.5)
Redundancy	8.6
Refinement	
R_{work} / R_{free} (%)	25.96/28.54
Average B-factor	84.2
Bond length rmsd (Å)	0.002
Bond angle rmsd (°)	0.478
Ramachandran plot (%)	
Favored region	94.10
Outlier region	0.0
PDB code	8X7N

1056 [a] Statistics for the highest-resolution shell are shown in parentheses.
1057

1058 **Supplementary Table 2. Strains, Recombinant DNA, and Oligonucleotides used in this**
1059 **study.**
1060

Strain	Source	Identifier
Escherichia coli S17-1 ATCC 47055	American Type Culture Collection	ATCC 47055
Escherichia coli S17-1 ATCC 47055 Δ*trbE*	This paper	N/A
Escherichia coli MG1655 Tn7::Cat	This paper	N/A
Escherichia coli MG1655 Δ*ompA* Tn7::Cat	This paper	N/A
Escherichia coli MG1655 Δ*ompC* Tn7::Cat	This paper	N/A
Escherichia coli MG1655 Δ*ompW* Tn7::Cat	This paper	N/A
Escherichia coli MG1655 Δ*rfaD*::Cat	Ting et al., 2020	N/A
Enterobacter cloacae ATCC 13047	American Type Culture Collection	ATCC 13047
Enterobacter cloacae ATCC 13047 Δ*icmF*	Whitney et al., 2014	N/A
Salmonella enterica subsp. *enterica* serovar Typhimurium str. LT2	Gift from Dr. Shu-Jung Chang	N/A
Escherichia coli DH5α	YB Biotech	Cat# XR-LYE678-80
Escherichia coli S17-1 λ pir	Lab collection	N/A
Escherichia coli BL21 pRIL (DE3)	Gift from Dr. Hung-Ta Chen	N/A
Yeast-Display Nanobody Library (NbLib)	Kerafast	Cat#EF0014-FP
E. coli-Display Nanobody Library	This paper	N/A

1061

Recombinant DNA	Source
pDSG_Null (pDSG323)	Glass and Riedel-Kruse, 2018
pDSG_Nb1 (pDSG372)	Glass and Riedel-Kruse, 2018
pDSG_NbIB10 (pDSG_Nb-Int)	Ting et al., 2020
pDSG_Nb-BamA	Ting et al., 2020
pDSG_Nb-TraN	This paper
pDSG_Nb-TraN-myc	This paper
pDSG_Nb-TraN_F47A/Y58A	This paper
pDSG_Nb-TraN_Y98A/L100A	This paper
pDSG_Nb-TraN_S105C	This paper

pDSG_Nb-TraN_S105C-myc	This paper
pDSG_Nb-TraN_H106C	This paper
pDSG_Nb-TraN_H106C-myc	This paper
pDSG_Nb-OmpA	This paper
pDSG_Nb-OmpC	This paper
pDSG_Ag1 (pDSG358)	Glass and Riedel-Kruse, 2018
pDSG_AgInt (Intimin full length)	Ting et al., 2020
pDSG_TraN	This paper
pET-Duet-1-His6_TraN^{surf}	This paper
pET-Duet-1-His6_TraN^{surf} / Nb-TraN	This paper
pET22b_Nb-TraN_His6	This paper
pET22b_Nb-TraN F47A/Y58A_His6	This paper
pET22b_Nb-TraN Y98A/L101A_His6	This paper
pET22b_Nb-TraN S105C_His6	This paper
pET22b_Nb-TraN H106C_His6	This paper
pET22b_Nb-OmpA_His6	This paper
pET22b_Nb-OmpC_His6	This paper
pET11a-GFP-avi	Gift from Jen-Hsuan Wei
pET22b_Nb-OmpA-GFP_His6	This paper
pET22b_Nb-OmpC-GFP_His6	This paper
pBAD18_OmpA	This paper
pBAD18_OmpC	This paper
pRE118_EcoliΔ*ompW*	This paper
pGenR	This paper
pAmpR	Choi et al., 2005
pTmpR	This paper
pKD4	Datsenko and Wanner, 2000
pKD46	Datsenko and Wanner, 2000
pCP20	Cherepanov and Wackernagel, 1995

1062

Primer	**Sequences (5'-3')**	**Identifier**
Library construction		
Yeast_Nb_F	TTATATTTTTTGATGGTGCG ACTAGACAGGTGCAGCTGC AGGAAAGCGGC	Mission Biotech
Yeast_Nb_R	CCCTTTTTTGCCGGACTGCA GTTATTAGCTGCTCACGGTC ACCTGGGTGCC	Mission Biotech
pDSG_Null_backbone_F	CTAATAACTGCAGTCCGGC AAAAAAGGGCAAG	Mission Biotech
pDSG_Null_backbone_R	TGTCTAGTCGCACCATCAA AAAATATAACCGC	Mission Biotech
Bacteria strain construction		
EcoliS17_ΔtrbE_F	CGCTCGACCCCGTTCCGCG AGAACACCAATAGCCAAGG GAAGCAATACCGTGTAGGC TGGAGCTGCTTCG	Mission Biotech
EcoliS17_ΔtrbE_R	CGTTGCGGGCTTCTTCTTGA AGATCAAGCCCTTGATCGT	Mission Biotech

	GTCTGCAAAACCATATGAATATCCTCCTTA	
TrbE_seqF	GTTCCGCGAGAACACCAATA	Mission Biotech
TrbE_seqR	GCGGGCTTCTTCTTGAAGAT	Mission Biotech
MG1655_ΔompW_F1	CATGAATTCCCGGGAGAGCTCCATGATGCCAATCTGTAC	Mission Biotech
MG1655_ΔompW_R1	ATTAAAAACGCTTTTTCATATCCGCTCC	Mission Biotech
MG1655_ΔompW_F2	TATGAAAAAGCGTTTTTAATTCCGCACAAAAAC	Mission Biotech
MG1655_ΔompW_R2	CGACGGATCCCAAGCTTCTTCTAGAAAAGTCGAGCATTATGAGATTG	Mission Biotech
MG1655_ΔompW_seq_F2	GTCCTGTACCAACATCACCG	Mission Biotech
MG1655_ΔompW_seq_R2	AGGTCATCGAAAGTACCGAG	Mission Biotech
MG1655_ΔompA_F	GAGGCTTGTCTGAAGCGGT	Mission Biotech
MG1655_ΔompA_R	GCGGAACACCAGCATACGC	Mission Biotech
MG1655_ΔompA_seq_F	CAATGCTTTCAGTCGTGAC	Mission Biotech
MG1655_ΔompA_seq_R	AACCATTCGGGCAAGACG	Mission Biotech
MG1655_ΔompC_F	GTTGCGAGTGAAGGTTTTGTTTTGAC	Mission Biotech
MG1655_ΔompC_R	GCGTCCAGTTGGGTCTGAATC	Mission Biotech
MG1655_ΔompC_seq_F	GAGGCATCCGGTTGAAATAG	Mission Biotech
MG1655_ΔompC_seq_R	GCGATAAACTTTGCGAGTCG	Mission Biotech
Plasmid construction		
pBAD18_MG1655_ompA_F	TGGGCTAGCGAATTCGAGCTCATGAAAAAGACAGCTATCGCG	Mission Biotech
pBAD18_MG1655_ompA_R	TGCATGCCTGCAGGTCGACTCTAGATTAAGCCTGCGGCTGAGTTAC	Mission Biotech
pBAD18_MG1655_ompC_F	TGGGCTAGCGAATTCGAGCTCATGAAAGTTAAAGTACTGTCC	Mission Biotech
pBAD18_MG1655_ompC_R	TGCATGCCTGCAGGTCGACTCTAGATTAGAACTGGTAAACCAGAC	Mission Biotech
NbtraN_myc_F	GGCGAACAGAAGCTGATCAGCGAGGAAGATCTGTAATAACTGCAGTCCGGCAA	Mission Biotech

NbtraN_myc_R	CTGATCAGCTTCTGTTCGCCACCGCCGCTGCTCACGGTCACCTG	Mission Biotech
SL1344_TraN_F	TTATATTTTTTGATGGTGCGACTAGAACAACAGAGGTCAGAACC	Mission Biotech
SL1344_TraN_R	CCCTTTTTTGCCGGACTGCATTATTACTTTACCTGCATCACCAGTGTCAGCGTGAACGTC	Mission Biotech
BamHI_TraN_surf_F	ACCATCATCACCACAGCCAGGATCCGACAACAGAGGTCAGAACC	Mission Biotech
NotI_TraN_surf_R	GTTCGACTTAAGCATTATGCGGCCGCTTACTTTACCTGCATCACCAGTGTCAGCGTGAACGTC	Mission Biotech
NdeI_NbOmpA/NbOmpC_F	CTTTAAGAAGGAGATATACATATGCAGGTGCAGCTGCAGGAAAG	Mission Biotech
XhoI_NbOmpA/NbOmpC_R	AGTGGTGGTGGTGGTGGTGCTCGAGGCTGCTCACGGTCACCTG	Mission Biotech
NbOmpA/NbOmpC_GFP_R1	TGCTCACGCTGCTGCTCACGGTCACCTG	Mission Biotech
NbOmpA/NbOmpC_GFP_F2	CGTGAGCAGCAGCGTGAGCAAGGGCGAG	Mission Biotech
XhoI_Nb-OmpA/Nb-OmpC_GFP_6His_R	AGTGGTGGTGGTGGTGGTGCTCGAGCTTGTACAGCTCGTCCATGCC	Mission Biotech
NdeI_NbtraN_F	GTATAAGAAGGAGATATACATATGCAGGTGCAGCTGCAGGAAAG	Mission Biotech
XhoI_NbtraN_R	CAGCGGTTTCTTTACCAGACTCGAGTTAGCTGCTCACGGTCAC	Mission Biotech
NbtraN_F47A/Y58A_F	GAACGCGAAGCCGTTGCCGGTATTACTGCTGGTAGTAGTACCGCTTATGCGGATAGCGTGAAAGGC	Mission Biotech
NbtraN_F47A/Y58A_R	ATCCGCATAAGCGGTACTACTACCAGCAGTAATACCGGCAACGGCTTCGCGTTCTTTGCCCGGCG	Mission Biotech
NbtraN_Y98A/L100A_F	TGCGCGGCTGCGCCGGCGGACGAAATCGGTTCTCATGAC	Mission Biotech
NbtraN_Y98A/L100A_R	GATTTCGTCCGCCGGCGCAGCCGCGCAATAATACACCG	Mission Biotech

NbtraN_S105C_F	GAAATCGGTTGCCATGACCCGCATTCTTATTGG	Mission Biotech
NbtraN_S105C_R	CGGGTCATGGCAACCGATTTCGTCCAGCGGGT	Mission Biotech
NbtraN_H106C_F	ATCGGTTCTTGCGACCCGCATTCTTATTGGGG	Mission Biotech
NbtraN_H106C_R	ATGCGGGTCGCAAGAACCGATTTCGTCCAGCG	Mission Biotech
NbcheckF	CTCTTGGGGCAAATAGTGCCAAA	Mission Biotech
NbcheckR	AGGAAGCCTGCATAACGCGAAG	Mission Biotech
pDSG_Nb1_seq_R	ACTACTAACGGTAACTTGCGTTC	Mission Biotech
pDSG_NbtraN_seq_R	ATGAGAACCGATTTCGTCCAGC	Mission Biotech
pBAD18_Seq_F	GCTATGCCATAGCATTTTTATCC	Mission Biotech
pBAD18_Seq_R	CTGATTTAATCTGTATCAGGCTG	Mission Biotech
pETDuet_MCS1_Seq_F	ATGCGTCCGGCGTAGA	Mission Biotech
pETDuet_MCS2_Seq_R	GCTAGTTATTGCTCAGCGG	Mission Biotech
pRE118 seq-F	GGTTGAGAAGCGGTGTAAGTG	Mission Biotech
pRE118 seq-R	GCAGGTCGATCCCAAGCTTC	Mission Biotech
MiSeq		
Nb_seq_UMI_offset_F1	TCGTCGGCAGCGTCAGATGTGTATAAGAGACAGNNNNNNNNCGGCAGCCTGCGCCT	Integrated DNA Technologies, Inc.
Nb_seq_UMI_offset_F2	TCGTCGGCAGCGTCAGATGTGTATAAGAGACAGNNNNNNNNNCGGCAGCCTGCGCCT	Integrated DNA Technologies, Inc.
Nb_seq_UMI_offset_F3	TCGTCGGCAGCGTCAGATGTGTATAAGAGACAGNNNNNNNNNNCGGCAGCCTGCGCCT	Integrated DNA Technologies, Inc.
Nb_seq_UMI_offset_F4	TCGTCGGCAGCGTCAGATGTGTATAAGAGACAGNNNNNNNNNNNACGGCAGCCTGCGCCT	Integrated DNA Technologies, Inc.
Nb_seq_UMI_offset_F5	TCGTCGGCAGCGTCAGATGTGTATAAGAGACAGNNNNNNNNNNNNACGGCAGCCTGCGCCT	Integrated DNA Technologies, Inc.
Nb_seq_offset_R1	GTCTCGTGGGCTCGGAGATGTGTATAAGAGACAGGCTGCTCACGGTCACC	Integrated DNA Technologies, Inc.

Nb_seq_offset_R2	GTCTCGTGGGCTCGGAGATGTGTATAAGAGACAGNGCTGCTCACGGTCACC	Integrated DNA Technologies, Inc.
Nb_seq_offset_R3	GTCTCGTGGGCTCGGAGATGTGTATAAGAGACAGNNGCTGCTCACGGTCACC	Integrated DNA Technologies, Inc.
Nb_seq_offset_R4	GTCTCGTGGGCTCGGAGATGTGTATAAGAGACAGNNNGCTGCTCACGGTCACC	Integrated DNA Technologies, Inc.
Nb_seq_offset_R5	GTCTCGTGGGCTCGGAGATGTGTATAAGAGACAGNNNNGCTGCTCACGGTCACC	Integrated DNA Technologies, Inc.

Figure 1.

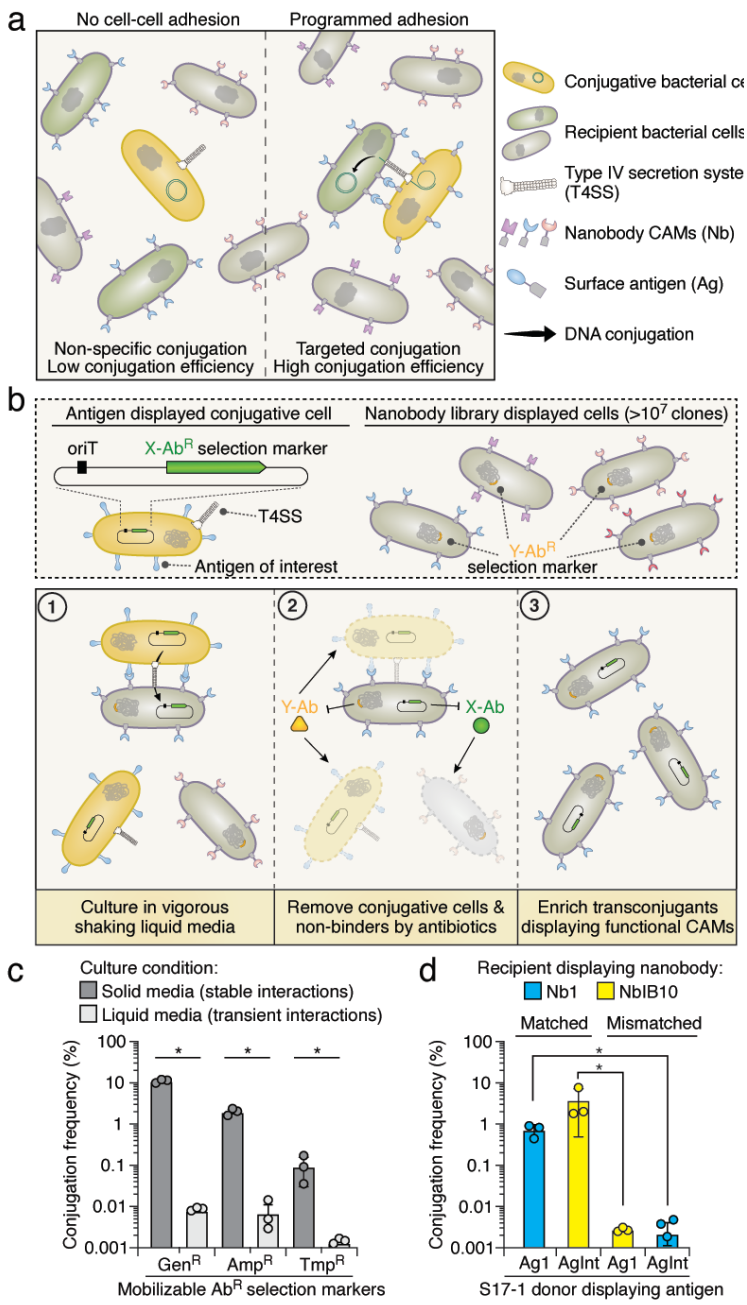

Fig. 1. Establishment of the whole-cell-based CAM discovery platform in liquid medium. (**a**) Schematic of the strategy for facilitating precise DNA conjugation between specific cells through synthetic cell-cell adhesion. Bacteria expressing diverse nanobodies (Nb) and conjugative cells with surface antigens (Ag) are involved. (**b**) The whole-cell-based selection platform is designed to identify nanobody CAMs targeting specific antigens of interest. Conjugative cells expressing the target antigen and cells displaying the nanobody library are employed. ① Within a liquid culture, contact-dependent DNA conjugation is enhanced through strong binding between cognate nanobodies and antigen pairs (both labeled in blue). ② After conjugation, antibiotics are used to eliminate conjugative cells and recipients expressing non-nanobody binders. ③ After a single round of selection, transconjugants carrying nanobodies with a relatively strong binding affinity toward the target antigens are enriched. (**c**) Conjugation frequencies (transconjugants/total recipients) of conjugative plasmids (pGenR, pAmpR, and pTmpR) were assessed under both solid and liquid growth conditions for a 6-hour duration. *E. coli* S17-1 serves as the conjugative donor strain, and MG1655 serves as the recipient strain. (**d**) Conjugation frequency of pGenR under the liquid growth condition. Recipient cells expressing nanobodies were co-cultured with donor cells displaying cognate or orthogonal antigens. Data are presented as means ± SD. n = 3 technical replicates, representative of two biological replicates. *$p < 0.05$, t-test. See also **Supplementary Fig. 1**.

1100 **Figure 2.**
1101
1102
1103
1104
1105
1106

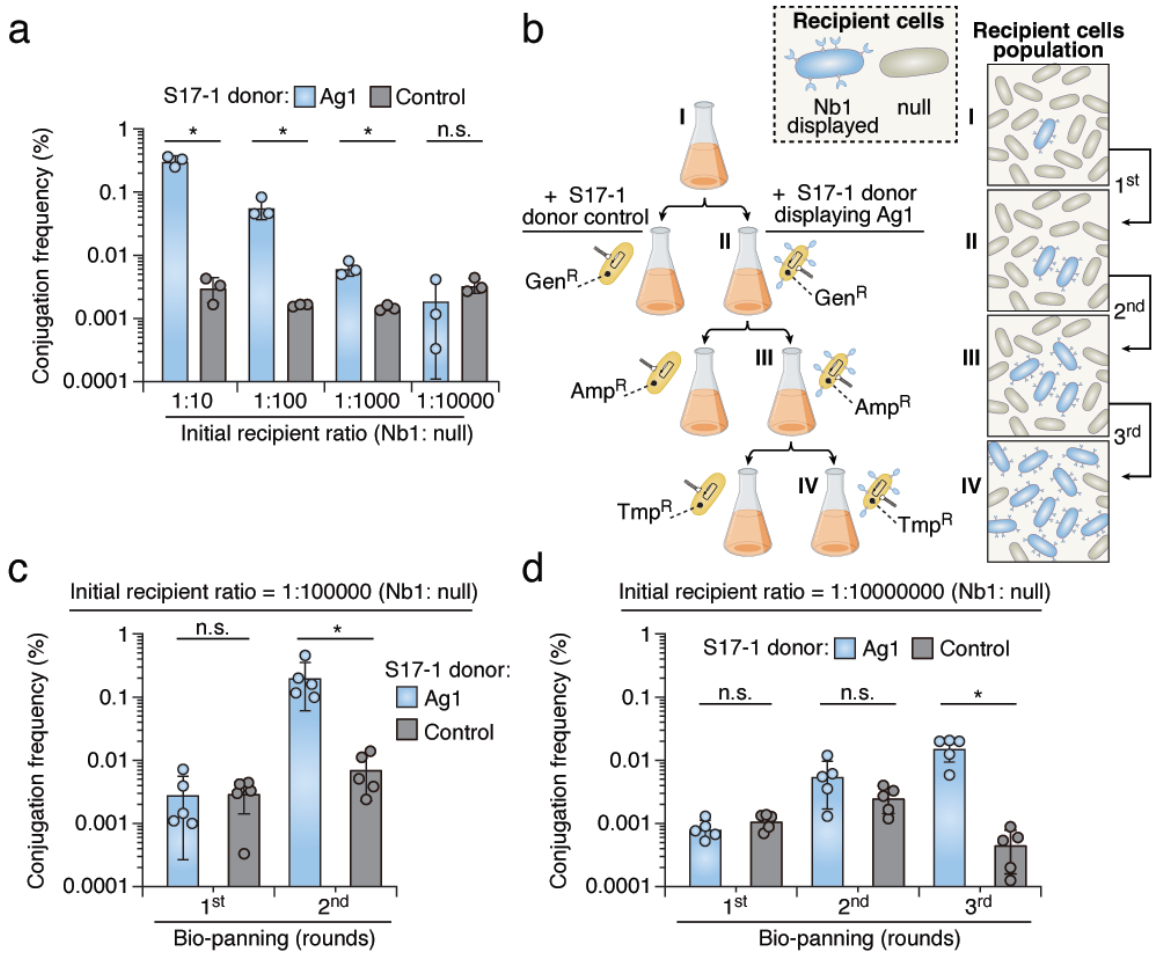

1107
1108
1109
1110
1111
1112
1113
1114
1115

Fig. 2. Iterative rounds of bio-panning enhance the discriminant capacity of the CAM selection platform. (**a**) Conjugation frequency of pGenR in conjugation assays within liquid culture between recipient and donor displaying Ag1 or Control (without antigen displayed). The recipient culture expressing Nb1 was 10-, 100-, 1000-, and 10000-fold diluted with the culture expressing non-matched null cells. (**b**) Schematic of three-round selection. For each round, donors (yellow) carry plasmids containing antibiotic-resistance genes against gentamicin (GenR), ampicillin (AmpR), or trimethoprim (TmpR) as distinct selection markers. The cartoon illustration on the right represents the progressive increase in the abundance of recipient cells displaying Nb1 (blue) in a mixed population with non-matched null cells (grey) during the selection process. (**c**) Conjugation frequency in two rounds of bio-panning. The initial population of recipient cells expressing Nb1 and null cells were mixed at a ratio of $1{:}10^5$. (**d**) Conjugation frequency in three rounds of bio-panning. The initial population of recipient cells expressing Nb1 and null cells were mixed at a ratio of $1{:}10^7$. Data are presented as means ± SD. n ≥ 3 technical replicates, representative of two biological replicates. *$p < 0.05$, t-test. See also **Supplementary Fig. 2**.

Figure 3.

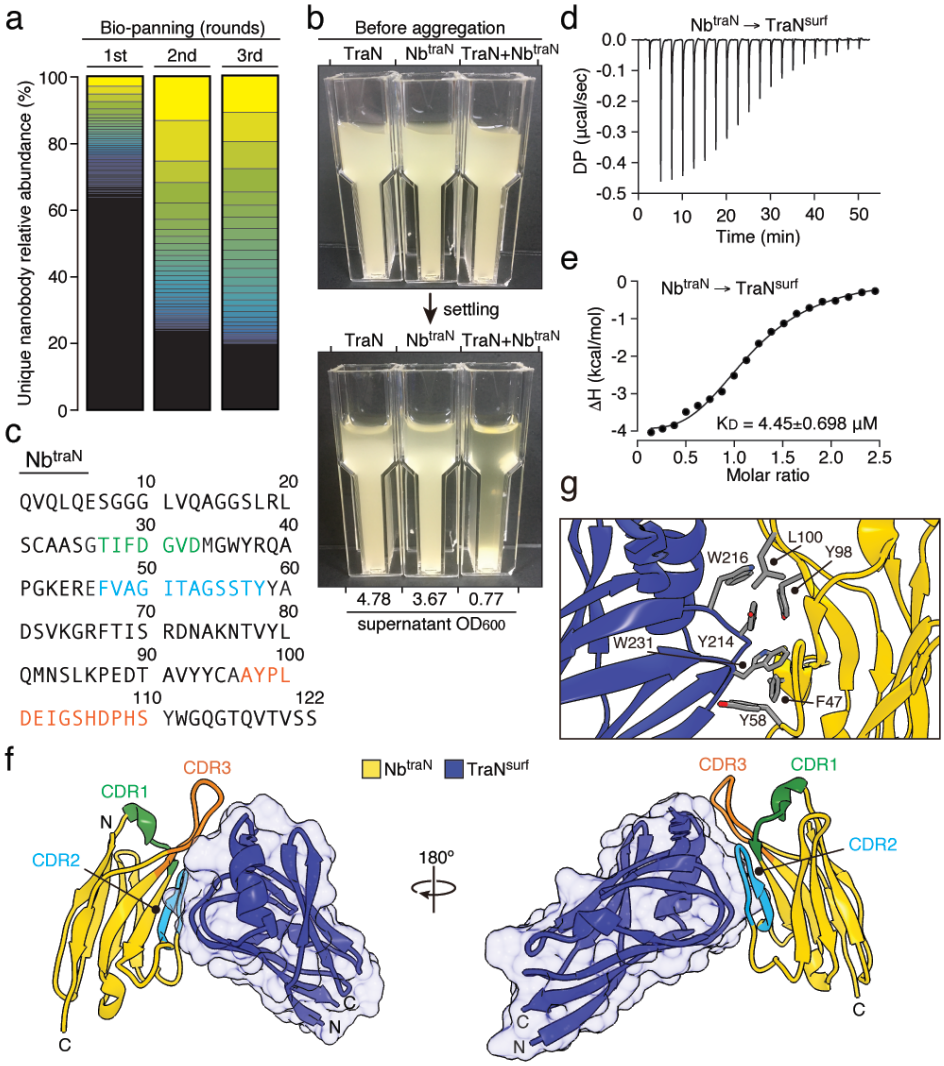

Fig. 3. Identification of nanobody recognizing TraN via the CAM discovery platform.
(**a**) Stacked bar plot illustrating the changes in the relative abundance of individual nanobodies within the population across three rounds of bio-panning to enrich for bacteria displaying TraN-binding nanobodies. Sequences were discerned through the CDR regions of the nanobody gene. The relative abundances of all unique nanobodies identified are shown, and the respective counts are detailed in **Supplementary Table 3**. Colors denote the ranking of nanobody abundance from the highest to lowest. (**b**) Macroscopic aggregation analysis to assess cell-cell adhesion. Cultures of *E. coli* strains displaying TraN or Nb^{traN} were incubated either individually or in combination. The OD_{600} of the supernatant after the settling period is shown below the image. (**c**) The amino acid sequence of Nb^{traN}, shows CDR1, CDR2, and CDR3 in green, blue, and orange, respectively. (**d, e**) The ITC binding profiles of Nb^{traN} with $TraN^{surf}$ at 25 °C. (**f**) Crystal structure of Nb^{traN} (yellow) in complex with $TraN^{surf}$ (blue) (PDB: 8X7N). CDR1, CDR2, and CDR3 are presented in green, blue, and orange, respectively. (**g**) A magnified view of the interacting residues is indicated between Nb^{traN} and $TraN^{surf}$. See also **Supplementary Table 1**.

Figure 4.

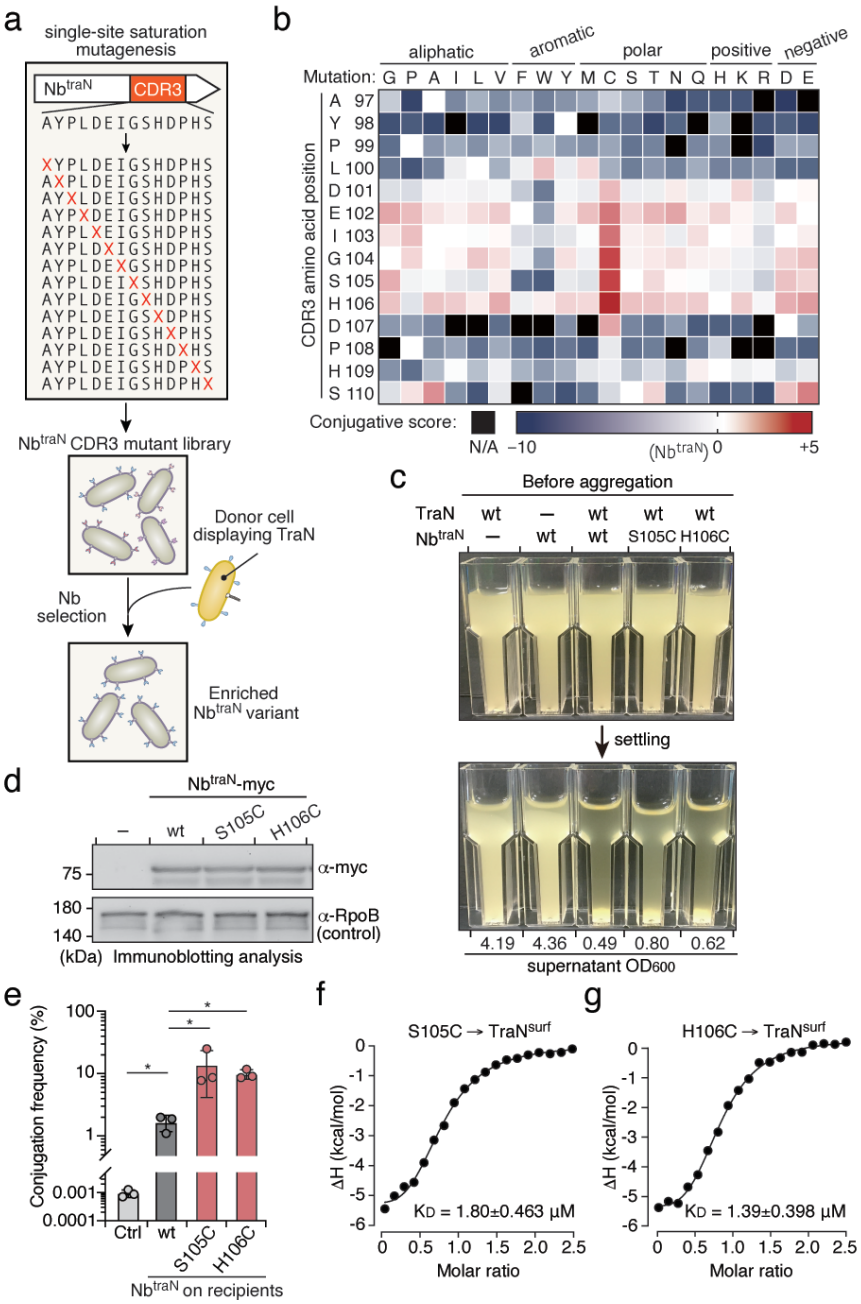

Fig. 4. Discovery of optimized Nb^{traN} variants through deep mutational scanning

(**a**) Selection workflow of the deep mutational scanning. Plasmids carrying Nb^{traN} genes with single-site mutations in CDR3 were utilized for library construction. The mutant library underwent a single round of selection with donor cells displaying TraN to enrich for bacteria expressing potent Nb^{traN} variants displaying stronger binding capacity. (**b**) The conjugative scores of individual Nb^{traN} CDR3 mutations are depicted in a heatmap. The X-axis represents individual amino acid mutation, and the Y-axis represents the residue position of CDR3 in wild-type Nb^{traN}. Mutations not identified after selection were excluded from the analysis and are shown in black (N/A). (**c**) Macroscopic aggregation analysis to assess cell-cell adhesion between *E. coli* strains displaying TraN and the indicated Nb^{traN} variants. The OD_{600} of the culture supernatant is shown below the image. The cells expressing TraN or wild-type Nb^{traN} were used as controls. (**d**) Immunoblotting analysis of *E. coli* expressing the Nb^{traN} variants carrying a C-terminal myc tag after a 16-hour incubation. The loading control is *E. coli* RNA Polymerase β protein (RpoB). Migrations of a size standard, in kDa, are indicted (left). (**e**) Conjugation frequency of pGenR under the liquid growth condition. Recipient cells expressing indicated nanobodies were co-cultured with donor cells expressing TraN. Data are presented as means ± SD. n = 3 technical replicates, representative of two biological replicates. *$p < 0.05$, t-test. (**f, g**) The ITC binding profiles of the indicated Nb^{traN} variants with TraN^{surf} at 25 °C. See also **Supplementary Fig. 5 and 6**.

Figure 5.

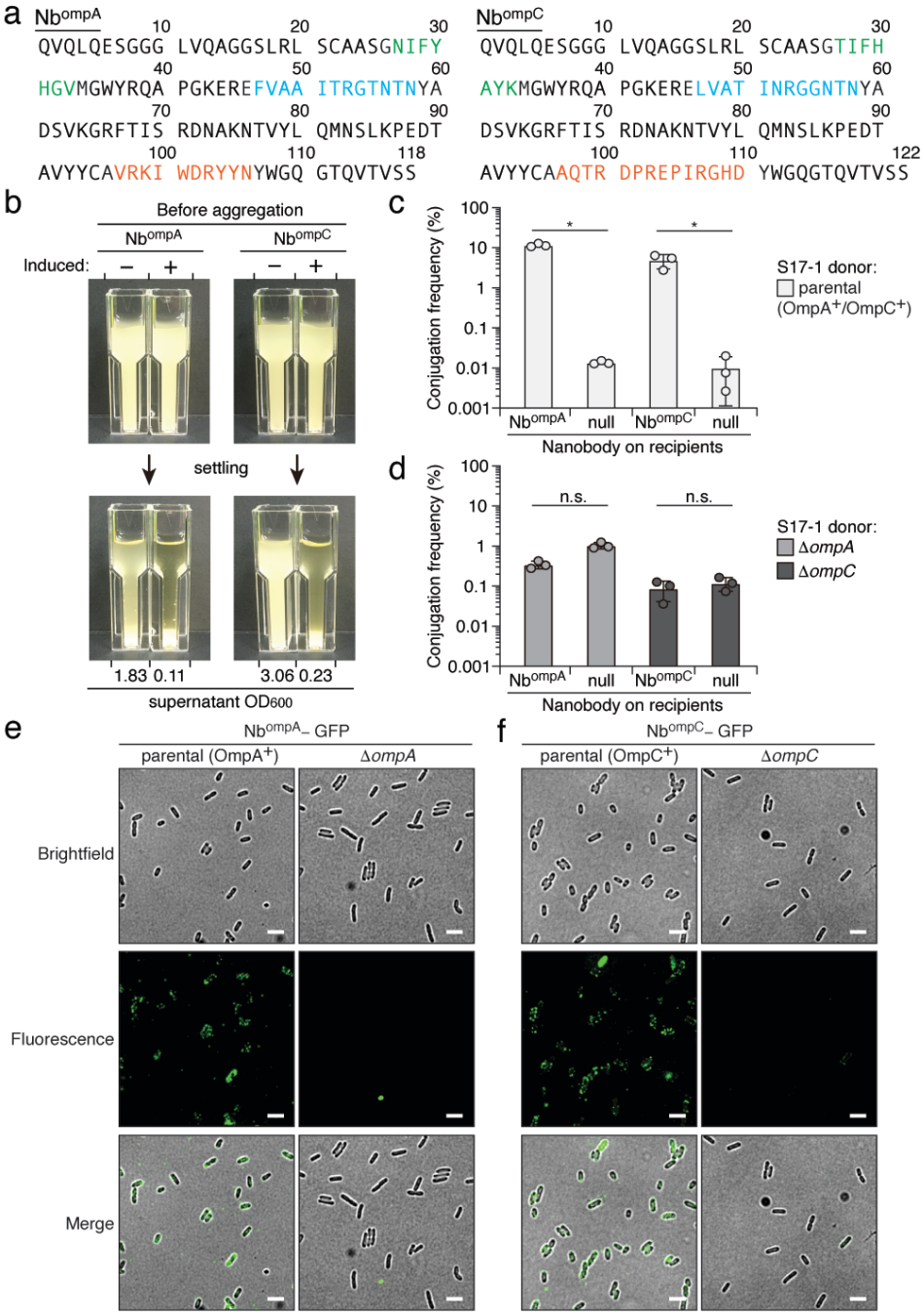

Fig. 5. Nanobody CAM targeting of *E. coli* integral membrane proteins OmpA and OmpC. (**a**) The amino acid sequence of Nb^{ompA} and Nb^{ompC}. CDR1 (green), CDR2 (red), and CDR3 (blue) are indicated. (**b**) Self-aggregation of *E. coli* expressing Nb^{ompA} and Nb^{ompC}. Cultures underwent 24-hour aTc induction before settling. Cultures that did not undergo induction (*i.e.,* not expressing nanobodies) are presented as controls. (**c, d**) Conjugation frequency of pGenR under the liquid growth condition. Recipient cells expressing indicated nanobodies were co-cultured with S17-1 donor cells expressing (**c**) or not expressing (**d**) the indicated antigens. Data are presented as means ± SD. n = 3 technical replicates, representative of two biological replicates. *$p < 0.05$, t-test. (**e, f**) Fluorescence micrographs showing the antigen-binding specificity of Nb^{ompA}-GFP (**e**) and Nb^{ompC}-GFP (**f**). Nb^{ompA}-GFP and Nb^{ompC}-GFP were incubated with wild-type *E. coli* and the antigen-deleted strains (Δ*ompA* or Δ*ompC*) for 1 hour before observation. Scale bar = 1 μm. Full-size images are available in **Supplementary Fig. 8**.

Figure 6.

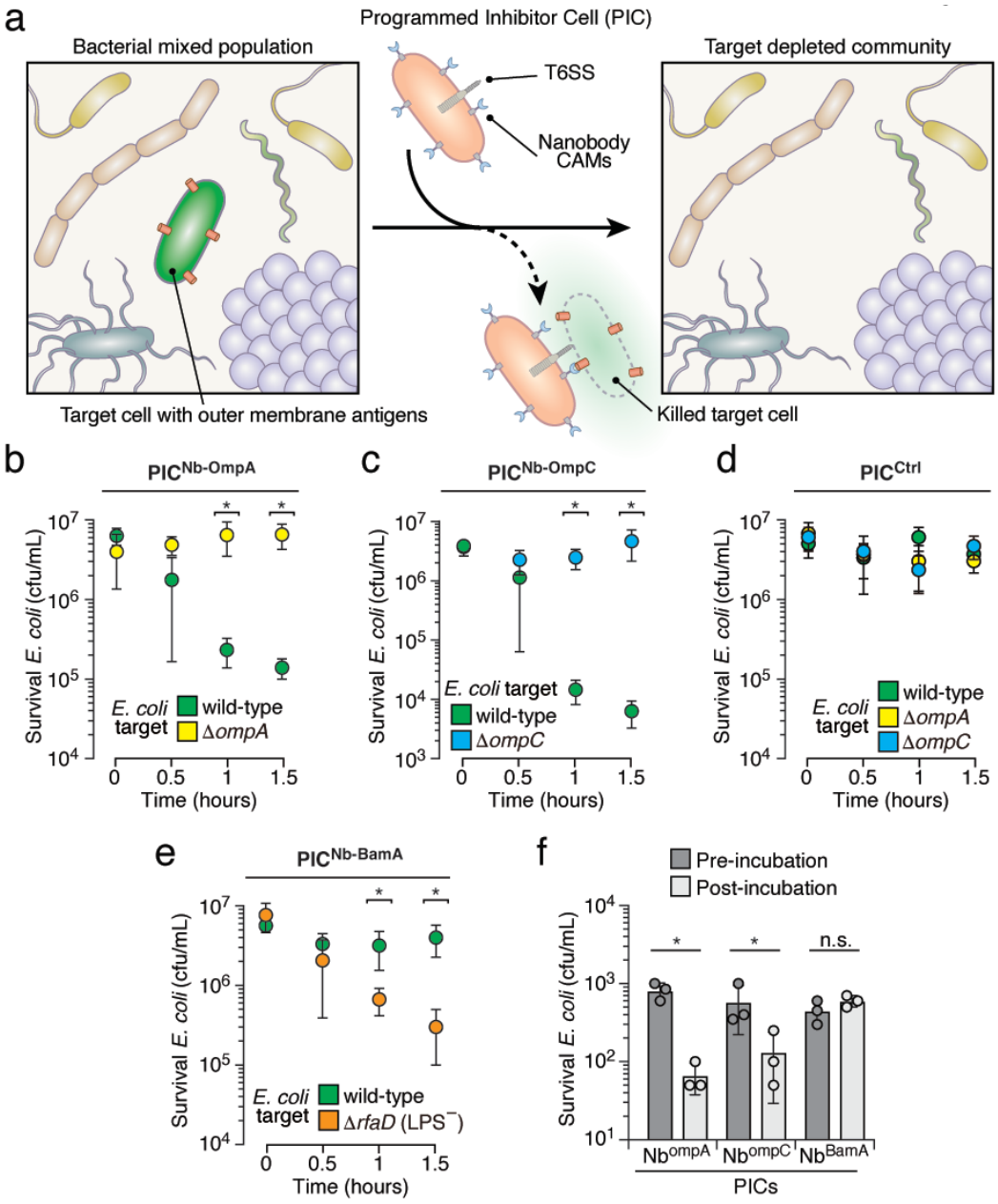

Fig. 6. Mounting Nb^{ompA} and Nb^{ompC} on PICs depletes target *E. coli* from bacterial mixtures. (**a**) Schematic of target depletion of bacteria (green) from a complex bacterial population by PICs (pink). (**b-e**) Survival (CFUs/mL) of *E. coli* strains (wild-type, Δ*ompA*, Δ*ompC*, and Δ*rfaD*, colored green, yellow, blue, and orange, respectively) upon incubation with PICs displaying Nb^{ompA} (**b**), Nb^{ompC} (**c**), non-match control (Ctrl) (**d**), or Nb^{BamA} (**e**) in liquid medium (n = 3 technical replicates ± S.D.; *$p < 0.05$, t-test). Two biological repeats were conducted. (**f**) Survival (CFUs/mL) of wild-type *E. coli* within a mouse fecal bacterial population before and after incubation with PICs displaying Nb^{ompA}, Nb^{ompC}, or Nb^{BamA} (n = 3 technical replicates ± S.D., representative of two biological replicates. *$p < 0.05$, t-test). See also **Supplementary Fig. 9 and 10**.

Supplementary Figure 1.

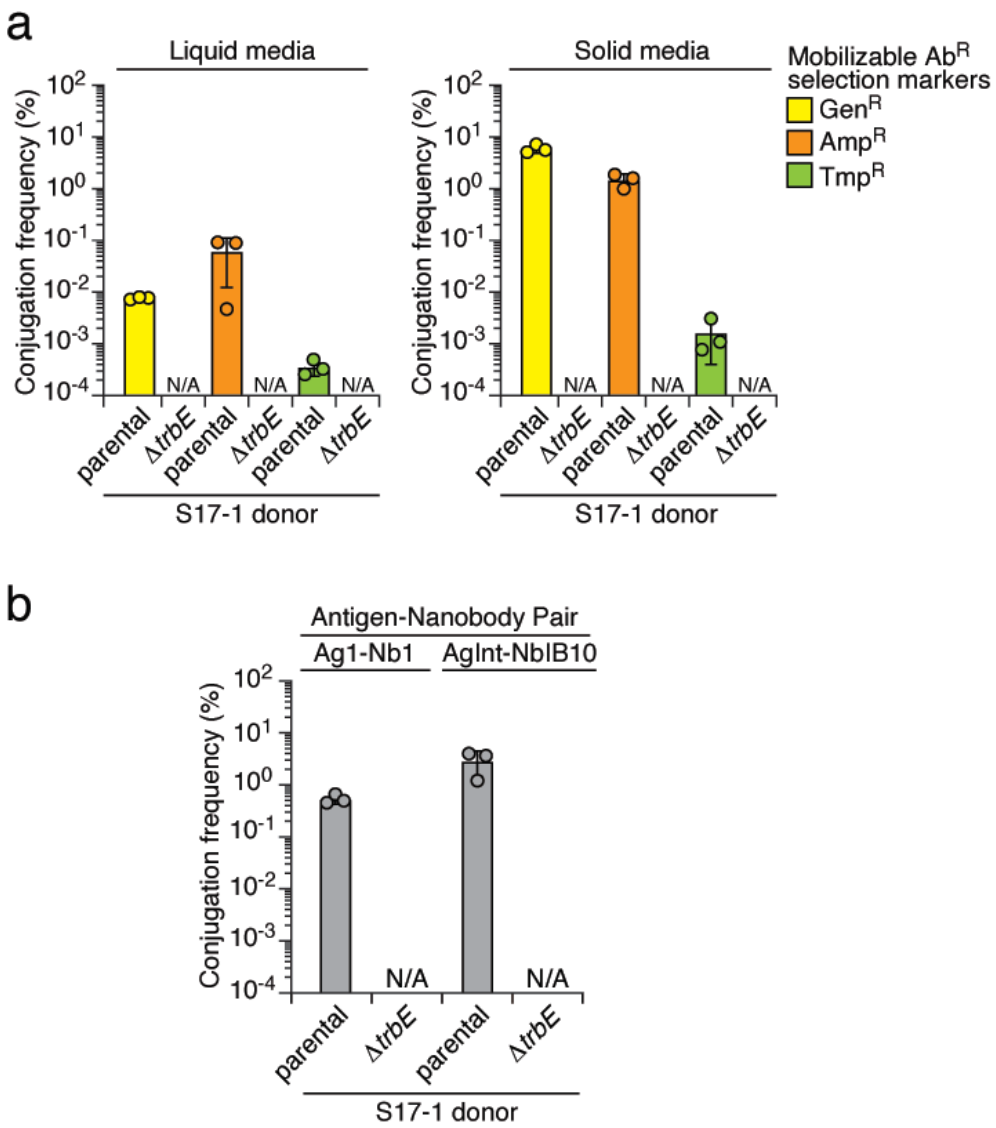

Fig. S1. Dependency of selection marker gene transfer on a functional T4SS.
(**a**) The conjugation frequency of selection markers from the WT and Δ*trbE* (dysfunctional T4SS) donors to recipients. Conjugation assays were performed under both liquid and solid growth conditions, utilizing pGenR, pCarbR, and pTmpR as selection markers. (**b**) The impact of a deficient T4SS on the donor (*E. coli* S17-1) to convey the selection marker (pGenR) to the recipient (*E. coli* MG1655). Two binding pairs were employed: Ag1 and AgInt were displayed by the donors, and their corresponding nanobodies (Nb1 and NbIB10) were displayed by the recipients. Data are presented as means ± SD. n = 3 technical replicates, representative of two biological replicates. *$p < 0.05$, t-test. Conjugation frequency lower than the detection limit designated as N/A.

Supplementary Figure 2.

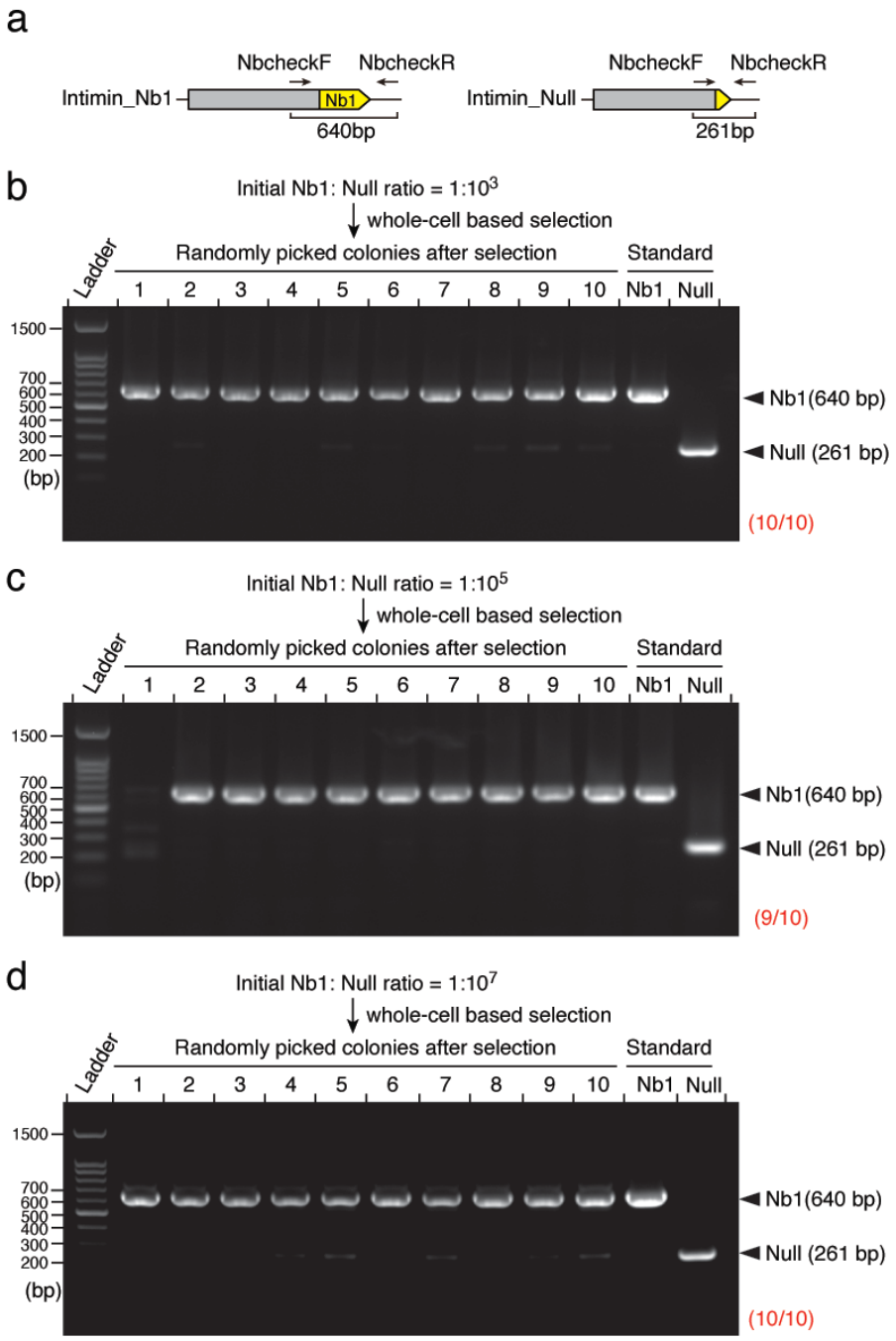

Fig. S2. Diagnostic PCR verification of the efficacy of the selection strategy in enriching for low-abundance nanobodies.

(**a**) The display system employed in this study comprises the intimin N-terminus (grey) fused with the adhesin region (yellow) at the C-terminus. Arrows indicate the annealing primers utilized for diagnostic PCR. The expected length of the PCR products for the cells displaying Nb1 (640 bp) and null (261 bp) are underscored. (**b**) PCR analysis of the transconjugants after selection. Two recipient strains expressing Nb1 and non-matched null control, respectively, were mixed at an initial ratio of $1:10^3$. The primers illustrated in (**a**) were used for diagnostic PCR. The proportions of colonies expressing Nb1 are denoted at the bottom-right (red). (**c**) Randomly selected colonies after two rounds of bio-panning were subjected to diagnostic PCR. The recipient cells displaying Nb1 were diluted with cells expressing a non-matched null control at an initial ratio of $1:10^5$. (**d**) The recipient population, initially at a ratio of Nb1:Null = $1:10^7$, after three rounds of selection was verified through diagnostic PCR.

Supplementary Figure 3.

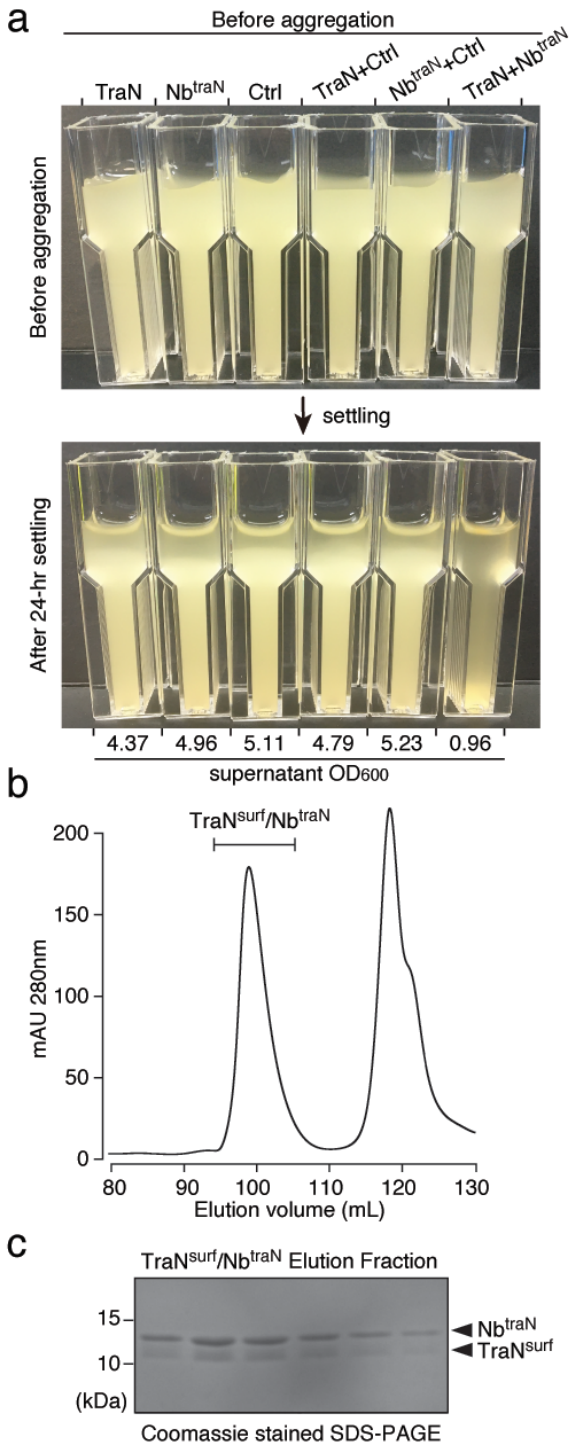

Fig. S3. Nb^{traN} binds to TraN.
(**a**) The macroscopic aggregation analysis to assess cell-cell adhesion for the indicated cultures of *E. coli* strains either individually or in combination. *E. coli* displaying TraN, Nb^{traN}, or the non-matched control (Ctrl) were tested. The OD_{600} of the culture supernatants was measured after the settling period. (**b**) Size-exclusion chromatography profile of the Nb^{TraN}/TraN^{surf} complex using a HiLoad 16/600 Superdex 200pg column. (**c**) The coomassie-stained SDS-PAGE protein gel shows the elution fractions of Nb^{traN} in complex with TraN^{surf}. Migrations of a size standard, in kDa, are indicted (left).

Supplementary Figure 4.

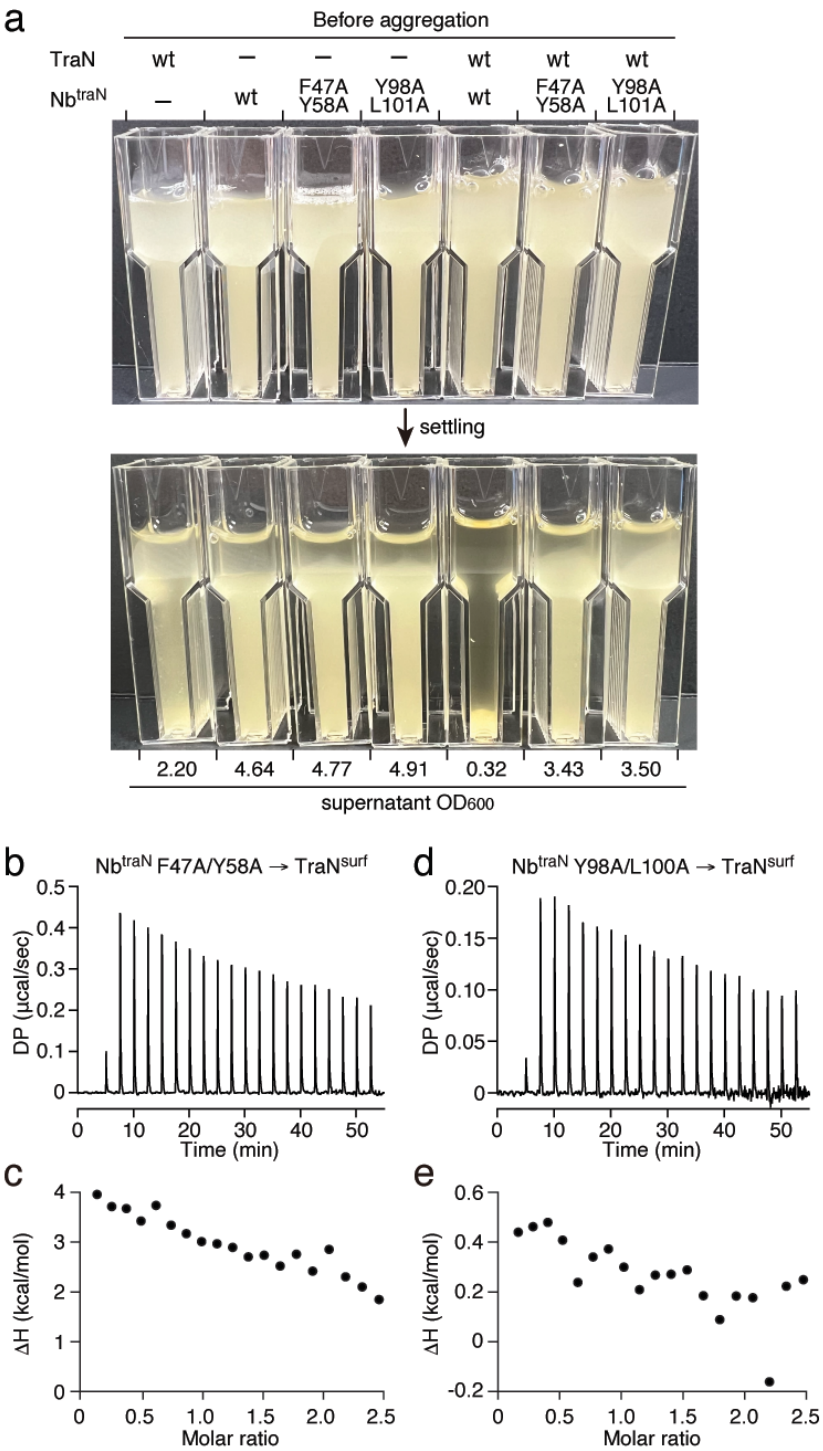

Fig. S4. Mutations in the CDR2 or CDR3 of Nb^{traN} affect its interaction with TraN.
(**a**) Comparison of the adhesive capability of the wild-type (wt) Nb^{traN} and its variants (CDR2: F47A/Y58A; CDR3: Y98A/L101A). For the macroscopic aggregation analysis, single cultures and mixtures were used. After settling, the OD_{600} of the culture supernatants was measured and values are shown below the image. (**b, c**) The ITC binding profiles of Nb^{traN} F47A/Y58A with $TraN^{surf}$. (**d, e**) The ITC binding profiles of Nb^{traN} Y98A/L101A with $TraN^{surf}$.

Supplementary Figure 5.

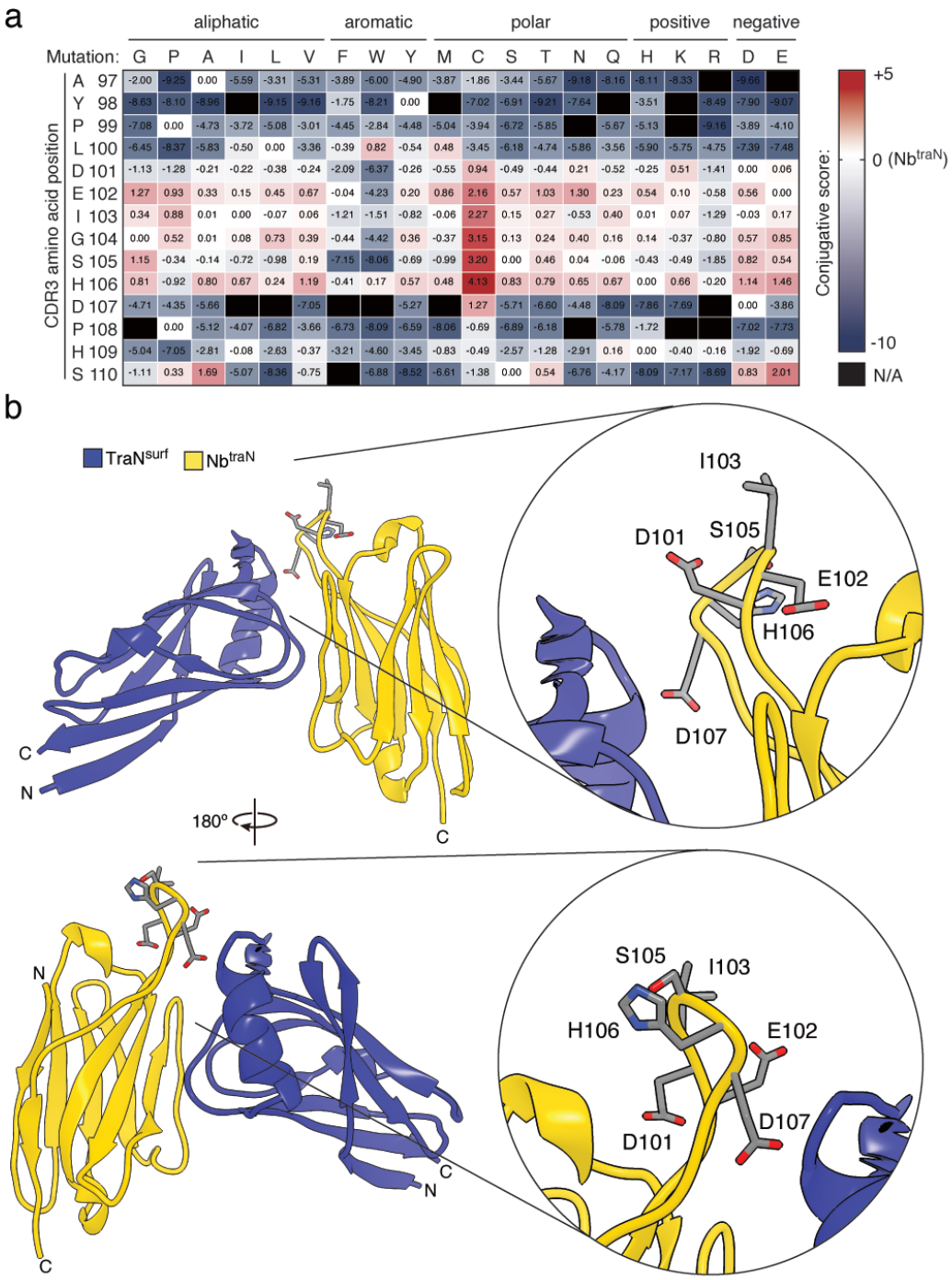

Fig. S5. Deep mutational engineering of CDR3 in Nb^{traN}.
(**a**) The values of the conjugative scores of single amino acid substitution within CDR3 of Nb^{traN}. Related to **Fig. 4**. (**b**) Crystal Structure of Nb^{traN} (yellow) bound to the surface-exposed domain of TraN (TraN^{surf}, blue) (PDB: 8X7N). A second view (rotated 180° around the vertical axis) is shown below. The close-up views on the right side indicate the locations of the cysteine variants (residues 101 to 107) on Nb^{traN}.

Supplementary Figure 6.

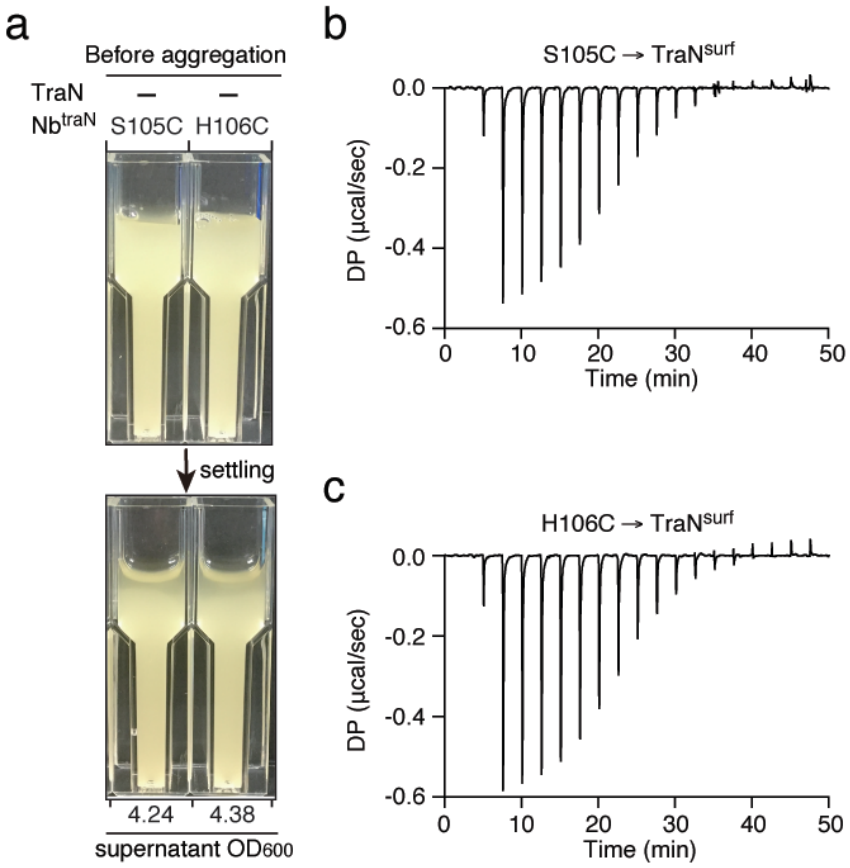

Fig. S6. Residue substitutions of CDR3 in Nb^{traN} improve its binding to TraN.
(**a**) Control cultures of *E. coli* strains expressing the Nb^{traN} variants that were used in the macroscopic aggregation assay in **Fig. 4**. (**b, c**) The ITC binding profiles of Nb^{traN} S105C (**b**) and H106C (**c**) with $TraN^{surf}$. Related to **Fig. 4**.

Supplementary Figure 7.

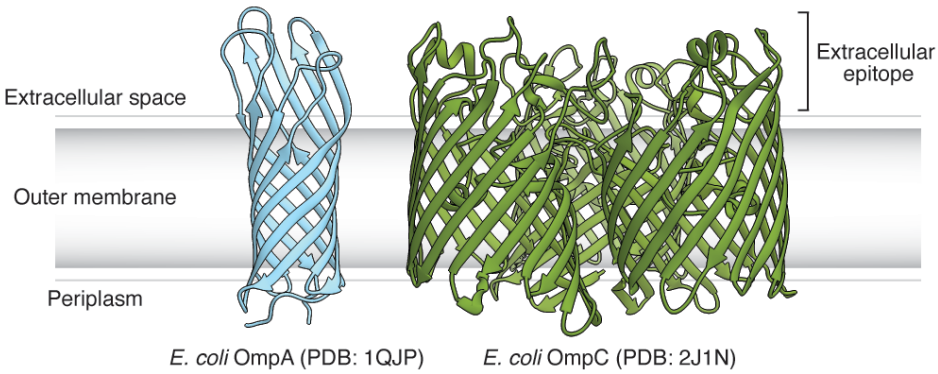

Fig. S7. Structures of *E. coli* OmpA and OmpC.
Crystal structures of the OmpA membrane domain (PBD: 1QJP)[1] and OmpC (PDB: 2J1N)[2] from *E. coli*. OmpA (blue) is presented as a monomeric structure, featuring an eight-stranded β-barrel spanning the outer membrane, coupled with flexible loops at its external end. Homotrimeric OmpC (green) is composed of three beta-barrels. The monomeric form of OmpC exhibits a 16-stranded β-barrel porin fold, with irregular extracellular loops.

Supplementary Figure 8.

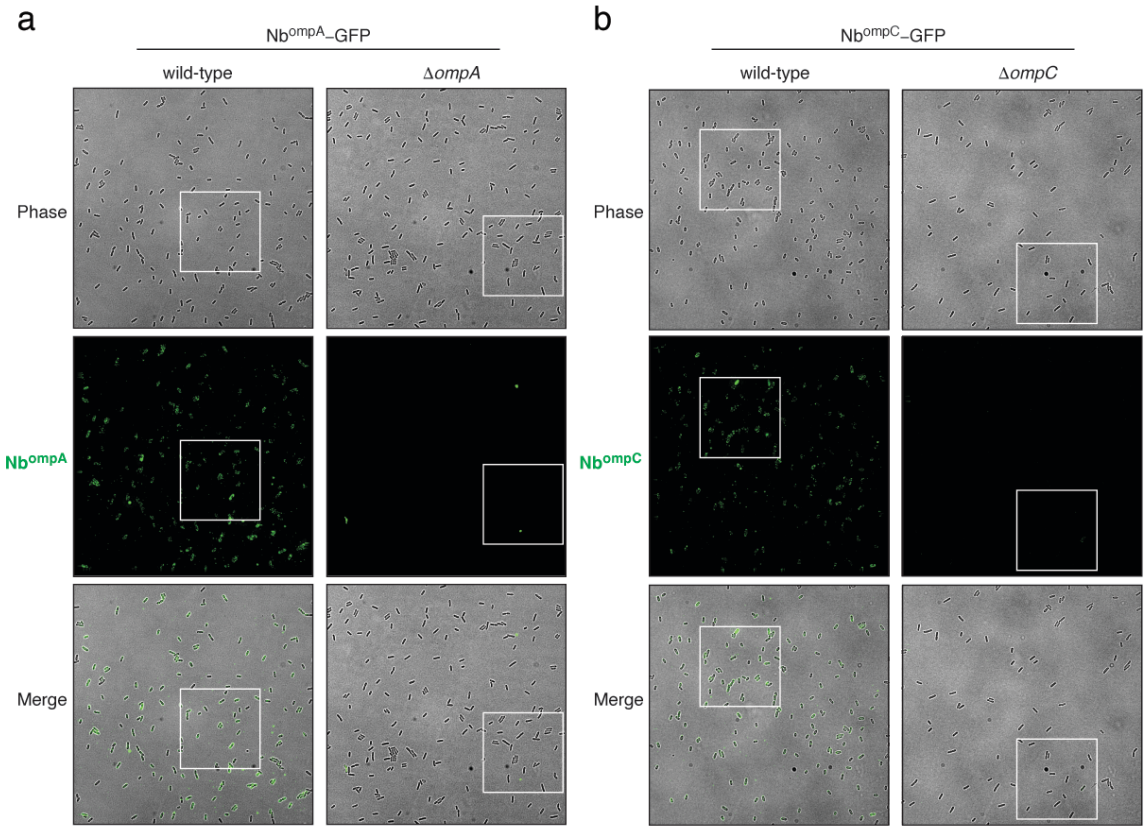

Fig. S8. Nb^{ompA}-GFP and Nb^{ompC}-GFP bind to their target antigens.
(**a**) The phase-contrast (top), green fluorescence (middle), and merged (bottom) images of *E. coli* (wild-type and *ΔompA* strain) following 1-hour incubation with Nb^{ompA}-GFP. The white borders demarcate the cropped images displayed in **Fig. 5e**. (**b**) Fluorescence micrographs of *E. coli* (wild-type and *ΔompC* strain) cells treated with Nb^{ompC}-GFP for 1 hour. Phase-contrast (top), green fluorescence (middle), and merged (bottom) images are presented. Zoomed-in images of the areas within white borders are featured in **Fig. 5f**.

1642 **Supplementary Figure 9.**

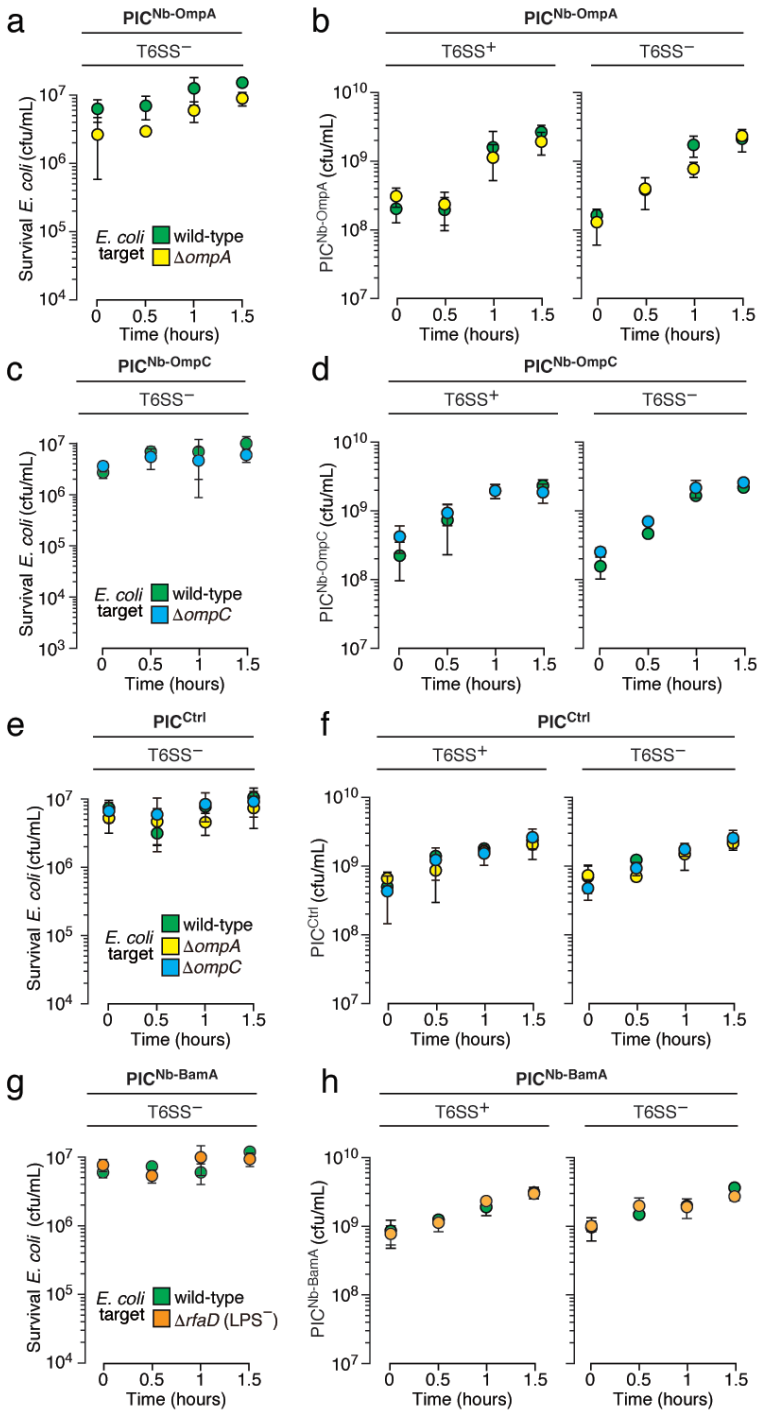

1643
1644
1645 **Fig. S9. Target depletion mediated by PICs requires a functional T6SS, and survival of PICs upon**
1646 **incubation with target *E. coli*.**
1647 (**a, c, e, g**) Survival (CFUs/mL) of *E. coli* MG1655 wild-type, Δ*ompA*, Δ*ompC*, and Δ*rfaD* strains (colored
1648 green, yellow, blue, and orange, respectively) upon liquid co-culture with T6SS-deficient PICs expressing
1649 Nb^{ompA} (**a**), Nb^{ompC} (**c**), non-matched control (**e**), or Nb^{BamA} (**g**). (**b, d, f, h**) The survival CFU of PICs
1650 expressing Nb^{ompA} (**b**), Nb^{ompC} (**d**), non-matching control (**f**), or Nb^{BamA} (**h**) upon liquid co-culture with target
1651 cells *E. coli* MG1655 wild-type (green), Δ*ompA* (yellow), Δ*ompC* (blue), and Δ*rfaD* (orange) cells. PICs with
1652 a functional (T6SS+) or dysfunctional T6SS (T6SS–, Δ*icmF*) were utilized. Data are presented as means ±
SD. n = 3 technical replicates, representative of two biological replicates. *$p < 0.05$, t-test.

1653 **Supplementary Figure 10.**
1654
1655
1656
1657

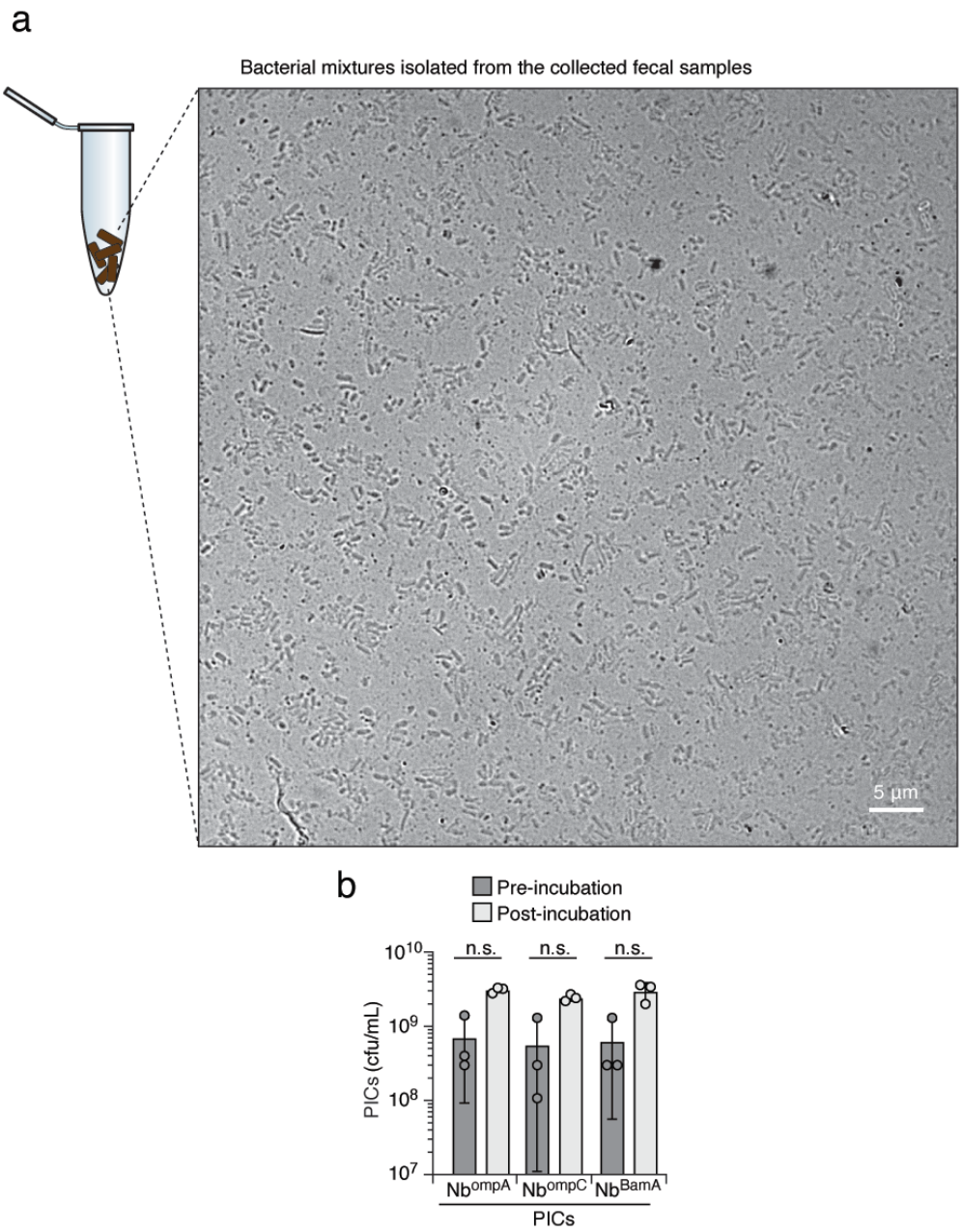

1693
1694
1695
1696
1697
1698 **Fig. S10. Survival of PICs remains unaffected before and after incubation in a**
1699 **bacterial mixture derived from mice fecal samples.**
1700 **(a)** Phase-contrast micrograph of a bacterial population isolated from mouse fecal samples.
1701 Scale bar = 5 µm. (**b**) Survival (CFUs/mL) of PICs before and after incubation with mouse
1702 fecal microbiota. Related to **Fig. 6f**.